Study on the application of carbon nanowalls for culturing osteoblasts

ICHIKAWA Tomonori

2022
Nagoya University
Graduate School of Engineering
Department of Electrical Engineering and Computer Science

Chapter 1 Introduction

1.1 Carbon nanomaterials

Carbon-based nanomaterials from zero-dimensional to three-dimensional structure such as fullerenes, carbon nanotubes (CNTs) and graphene sheets, have attracted much attention in diverse research fields since their discoveries. [1)]

Fullerenes are nanomaterials in which carbon atoms from a spherical network structure. Buckminsterfullerene (C_{60}) is the typical molecular crystal of fullerene which structured by 60 atoms of carbon atoms and its icosahedral symmetry cage like structure is composed of twenty hexagonal rings and twelve pentagonal rings. The diameter of C_{60} is about 0.7 nm. It is predicted by Osawa in 1970, and discovered by Kroto et al. in 1985. [2),3)]

CNTs are nanomaterials which is a cylindrical structure formed with rolled up graphene sheets. There are two kinds of CNTs, the multi-walled CNTs (MWNTs) consisted of up to several tens of graphitic shells is discovered by Iijima in 1991, and The single-walled carbon nanotubes (SWNTs) is discovered by Iijima, Ichihashi and Bethune et al.in 1993. [4)–6)] The CNTs have some features such as high aspect ratio, high mechanical strength and high conductivity due to its structure.

Graphene is a sheet of single atomic plane of graphite with a two-dimensional honeycomb lattice. This is a basic structural unit for various carbon-based nanomaterials including fullerenes and CNTs.

1.2 Carbon nanowalls (CNWs)

CNWs are self-organized carbon nanomaterials with a wall-like aggregation of nanographene oriented vertically on a substrate as shown in Fig. 1.2.1. CNWs is developed by Wu et al. and Hiramatsu et al. in 2004.[7),8)]

Thickness of each wall of CNWs is a few nanometers and a height is controllable in the order of micrometeres.[8),9)] CNWs have superior features, such as high aspect ratio, highly specific surface area, surface modification of chemical termination, and high electrical and thermal conductivity. Furthermore, CNWs maintain the structure and high mechanical strength that inhibits to aggregate even under high surface tension in liquids. Due to these characteristics, CNWs are expected to have various applications, such as electrodes of fuel cells and electron emission sources. [8)–21)]

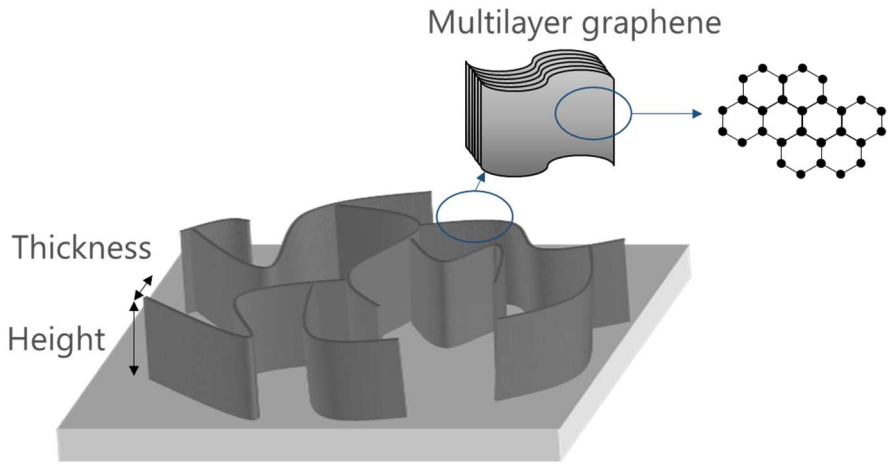

Fig. 1.2.1 Illustration of CNWs

1.3 Bone cells and osteoblasts

1.3.1 Diseases by a decrease in osteoblasts

The osteoporosis is serious problem among bone diseases. The number of osteoporosis patients exceeds 10 million in Japan and one in three of the women over the age of 50 suffers from it. Bone is formed by the osteoblasts. However, it has been reported that the osteoblasts decrease with age, and with alcohol and tobacco. [22)–25)]

Many researchers reported that bones play an important role in addition to the function of supporting the body.

Oury et al. reported about the effect of the osteocalcin (OC) on mice's memory. They investigated the dependency of the arrival time at the islands in the pool on the number of trials when the mice were placed in the pool. [26)] According to this report, the arrival time of mice with OC improved as the number of trials increased, whereas the arrival time of mice knocked out of OC generation worsened as the number of trials increased. Furthermore, administration of OC to knockout mice showed a decrease in arrival time due to an increase in the number of trials. These results indicate that OC is a protein required for animal memory.

Mera et al. reported about the effect of OC on muscle. [27)] According to this report, mice knocked out of OC have reduced muscle strength compared to wild-type mice, and administration of OC to knockout mice restores muscle strength of mice. These results indicate that OC is essential for maintaining muscle strength.

Thus, the function of the bones in our body attracted attention because these results have been confirmed in mice experiments. It is thought that the decrease in osteoblasts due to aging and lifestyle not only reduces bone density, but also reduces the amount of OC produced, leading to a decrease in memory and muscle strength. Therefore, a cell response control method for proliferation and differentiation is required in order to efficiently obtain osteoblasts and increase bone density and OC production.

1.3.2 Role of osteoblasts

There are osteoblasts, osteoclasts and bone cells in the bone. The osteoblasts make bone and osteoclasts destroy the old bone to metabolize it. The osteoblasts differentiate bone cells that become a part of bone and no longer proliferate. Fig. 1.3.1 shows the role of the osteoblasts. The osteoblasts proliferate without differentiation.

However, they differentiate to bone cells and stop to proliferate. In general, during differentiation, a large amount of run-related transcription factor 2 (Runx2) which is a transcription factor is produced in cells and the expression level of OC, which is a non-collagen protein of bone is increased. OC is released extracellularly to form bone. Also, the amount of extracellular calcium increases as osteoblasts differentiate. Therefore, Runx2, OC and the amount of extracellular calcium are used as indicators of differentiation of osteoblasts.

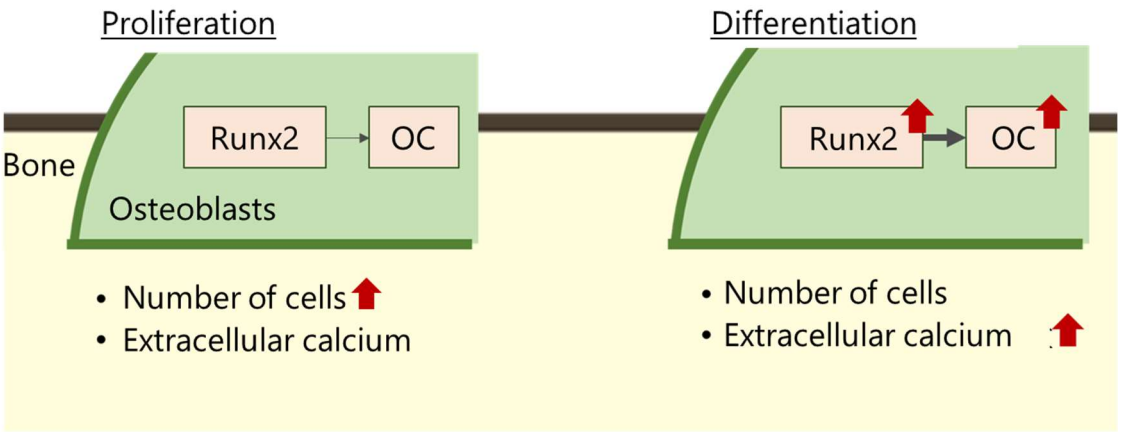

Fig. 1.3.1 The functions of osteoblast

1.4 Regulation of the cell response

Cell's functions are controlled by stimulation, such as the structure and elasticity of the scaffold, adherence of cells, external stimulation by electricity, electromagnetic fields, light, non-ionizing radiation, and ultrasonic sound waves. Also, there is an intracellular stimulus that introduces genes and cell growth factors into the cell. [28] This section describes the cell function control method, especially for controls of scaffolding and electrical stimulations.

1.4.1 Effect of scaffold on culturing cells

The cells are seeded on the culture scaffold, adhere to the scaffold, and then proliferate and differentiate. Adhesion to the scaffold always occurs first in this culture, and since the characteristics of the scaffold have an important role in the cell behavior. The regulation methods of proliferation and differentiation of cells have been widely studied by changes of scaffolds. The following studies have been reported that cell behavior is affected to scaffold properties, such as elasticity, wettability and micro-nano scale structures. [29)–37)]

- Neural stem cells (NPC cells) grew efficiently on a scaffold with regularly arranged collagen nanofibers than with randomly arranged collagen nanofibers. [29)]
- Regularly arranged poly-L-lactic acid (PLLA: Poly-L-lactide) scaffolds promoted the differentiation of bone marrow stromal cells into bone cells. [30)]
- Oriented poly-ε-caprolactone / poly-L-lactic acid / nano-hydroxyapatite (PCL / PLLA / nano-HA) complex scaffold increased the rate of induction of differentiation of human unrestricted somatic stem cells (hUSSC) into bone lineage cells. [31)]
- In culturing human mesenchymal stem cells (hMSC) on hydrogel, the uneven structure promoted the differentiation into bone line cells, and the hexagonal structure promoted the differentiation into adipose-producing line cells. [33)]
- The cells were regulated the extension area and differentiated differently by changing the area of the scaffold. [34)]
- In culturing MSCs using the elasticity of the scaffold, MSCs were cultured on a gel scaffold using collagen-I, which could change the elastic force. When the elastic force was 0.1 k to 1 kPa, it became a nervous system cell; 8 k to 17 kPa differentiated into myoblasts; 25 k to 40 kPa differentiated into bone cells. [35)]

1.4.2 The effect of electrical stimulation (ES) on cultured bone cells

The electrical stimulation (ES) has been used to treat bone. [38)–43)] The following studies have been reported.

- ES promoted the calcification of osteoblast-like cells cultured on the dish. [44)]
- ES promoted the proliferation of human fetal osteoblast (hFOB) cultured on a titanium oxide nanotube scaffold. [45)]
- ES promoted the proliferation and differentiation of Saos-2 cells cultured on a scaffold complexed Polylactic acid and Carbon nanotube (PLA/CNT). [46)]

There are several methods for ES applied to cells, such as (a) the parallel plate type that prepares an upper electrode and uses the scaffold as the lower electrode, (b) the parallel plate type that prepares two electrodes vertically standing on the scaffold, (c) applying the current only to the scaffold (d) applying the electromagnetic field as shown in Fig. 1.4.1.

The method of (c) is possible to apply only electromagnetic field to cells since the electrolysis of the medium is unlikely to occur compared to the methods of (a), (b), and (d). Meng et al. reported that the differentiation of Saos-2 cells cultured with current stimulus applied only to scaffold on Poly-L-lactide / Polypyrrole / heparin (PLLA/PPy/HE). [47)]

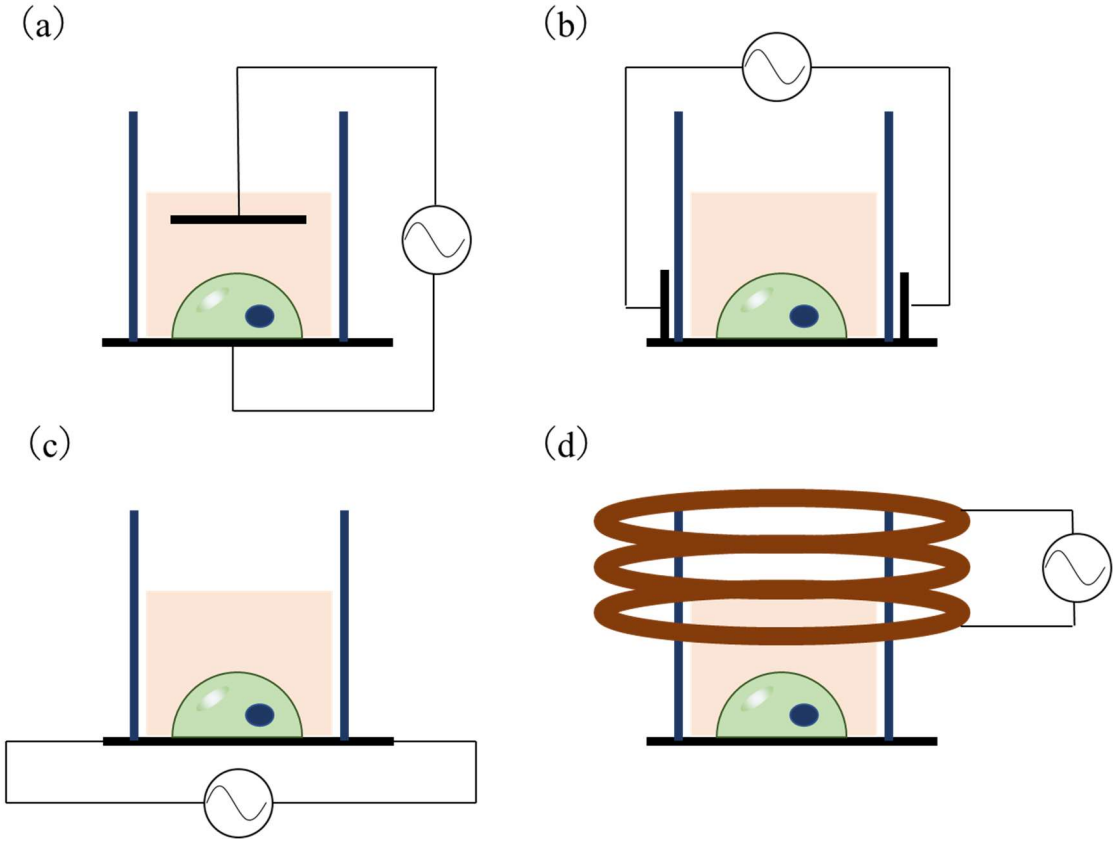

Fig. 1.4.1 The method of applying ES for cultured cells

1.5 Carbon nanomaterials for scaffold application to culture cells

1.5.1 Carbon nanomaterials for scaffold

The application of carbon nanomaterials for scaffold has a potential of the ES-purposed scaffolds, because of its biocompatibility, nano-micro structure and conductivity. For example, Regularly arranged carbon nanotubes (CNTs) scaffolds increased the proliferation of hMSCs and the rate of induction of differentiation into bone cells. [32)]

1.5.2 CNWs scaffold for scaffold application

The characteristics of CNWs for culturing cells are expected as shown in Fig. 1.5.1.

① Unique morphology of cells adhered on the CNWs edges.
② Chemical controllability of the scaffold with changing the chemical termination of the edge of CNWs.
③ Physical controllability of the scaffold with changing the wall-to-wall distances.
④ Culturing cells with application of ES due to highly conductive scaffolds.

Some researchers reported about the effect of chemical termination of CNWs scaffold on behavior of cells.

Watanabe et al. reported about the proliferation rate and spreading cell ratio of HeLa cells cultured on CNWs scaffold.[12)] CNWs were prepared using a radical injection plasma-enhanced chemical vapor deposition (PECVD) system with H_2 and CH_4 gases, and chemical terminations of CNWs were modified by plasma treatments of gases, such as hydrogen, oxygen, nitrogen and fluorine. This report indicates that CNWs have a biocompatibility for culturing Hela cells and the proliferation rate of Hela cells is not affected to the chemical termination of CNWs.

Stancu et al. reported about the effect of chemical termination of CNWs scaffold on attachment of fibroblast-like cells. [48)] CNWs were prepared using a PECVD system with Ar, H_2 and C_2H_2 gases. The chemical terminations of CNWs were modified by plasma generated in argon admixed with ammonia or nitrogen. This report indicates that the nitrogen-terminated CNWs are effective for the attachment of fibroblasts.

CNWs scaffold has not evaluated thoroughly yet for regulation of proliferation and differentiation of osteoblasts. Only features of the CNWs scaffold in terms of the chemical termination of CNWs were reported and there is no report about the evaluation

of CNWs as a conductive scaffold for applying ES, and the effect of wall-to-wall distances on differentiation of cells.

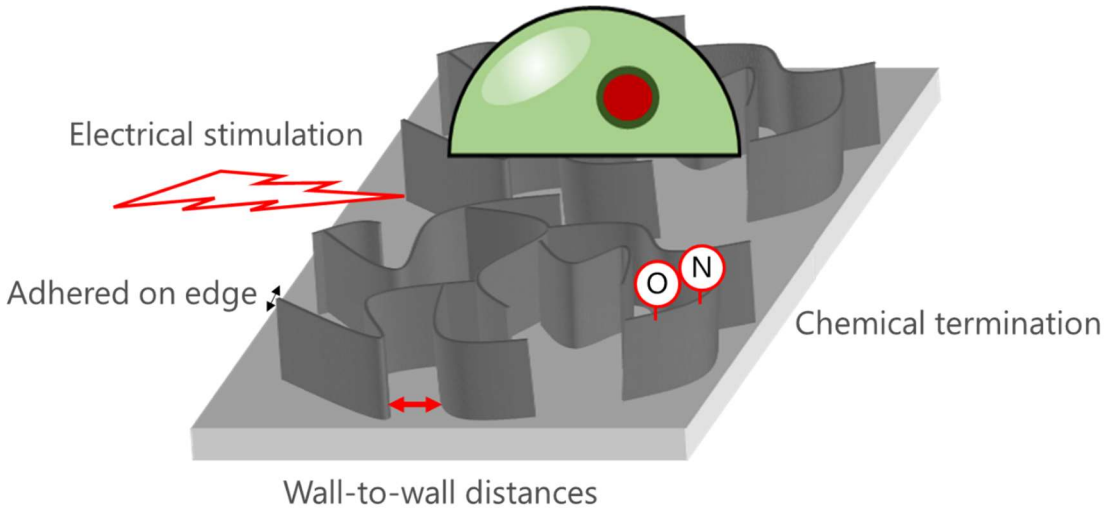

Fig. 1.5.1 Feature of CNWs for culturing cells

1.6 Objective and composition of this thesis

Nanomaterials for the scaffold applications to culture cells were studied by several researchers. The researches on scaffold application of the CNWs are limited in the applications for culturing osteoblasts. Herein, objective of this thesis is to clarify and discuss about a potential of three-dimensional structured CNWs for scaffold applications for culturing osteoblasts.

In Chapter 1, backgrounds of regenerative medicine and scaffold to culture cells are explained in detail. The explanations about the method of regulating cells including its background are described in Chapters 1.1, 1.2 and 1.3. The explanations about CNWs including its background, structure, characteristic, and the advantage of the application for scaffold are described at Chapter 1.4. Then the objective and composition of thesis are described in the Chapter 1.5.

In Chapter 2, the explanations on CNWs synthesis, culturing of cells and its evaluation methods are described. In Chapter 2.1, synthesis methods and descriptions about the CNWs deposition chamber, the radical injection plasma enhanced chemical vapor deposition system, and the evaluation methods for plasma emission, morphological and crystallographic of CNWs are explained. The explanations about methods culturing cells and methods for evaluation of morphology, proliferation and differentiation of cells are described in Chapter 2.2.

In Chapter 3, the effect of ES on proliferation and bone formation by osteoblast-like cells cultured on CNWs scaffolds is explained. Also, the effect of CNWs scaffold on cell morphology is described in Chapter 3.3.

In Chapter 4, the effect of wall-to-wall distances of CNWs on proliferation and gene expression of osteoblast-like cells cultured on CNWs scaffolds with ES is explained. Preparation of CNWs scaffolds with different wall-to-wall distances are described in Chapter 4.2. The effect of CNWs with different wall-to-wall distances and ES on proliferation, differentiation and morphology of cells are described in Chapter 4.3.

In Chapter 5, the effect of high-voltage nanosecond pulses on synthesis of sparsely isolated CNWs is described. Chapter 5.2 explains about fabrication of CNWs using high-voltage nanosecond pulses. Then, voltage and current characteristics of high-voltage nanosecond pulses during CNWs synthesis are described. The evaluation of the morphology of synthesized CNWs is described in Chapter 5.3. Finally, the mechanism of the isolated CNWs growth is discussed in Chapter 5.4.

In Chapter 6, the effect of isolated CNWs scaffold on cells behavior is described. The wall-to-wall distances of CNWs dependence on cells behavior is described in Chapter 6.3. Discussion about the relation of wall-to-wall distances and cells behavior, especially, differentiation and morphology, are expressed in Chapter 6.4.

Finally, in Chapter 7, all the results and discussions on CNWs scaffold applications are summarized. Scopes for future works on scaffold applications of CNWs are also addressed.

Chapter 2 Experimental setup and evaluation methods

2.1 Synthesis and evaluation method of CNWs

2.1.1 Radical injection plasma-enhanced chemical vapor deposition (RI-PECVD) system

When precursor gas is introduced in low pressure and the electric field is applied it, free electrons are accelerated by the electric field, and the electrons collide with the gas molecules. The collision is followed by the generation of a greater number of high energy electrons. The collisions of these electrons with the gas molecules promote reactions, such as excitation, dissociation and ionization, of the gas molecules, producing the chemically active species, such as excited states, radicals, and ions, at the room temperature. These radicals and ions are absorbed on the surface of substrate, proceed the surface chemical reactions and leading to the deposition and synthesis of thin films with formation of chemical bonds. This method is called the plasma enhanced chemical vapor deposition (PECVD) method. Compared to the thermal CVD, the PECVD has the advantages of lower temperature deposition which can be applied for plastic substrate. The PECVD can apply for thin-film solar cells applications and flat-panel display applications. In addition, the PECVD can be also used for the film deposition of polymer and diamond, and the synthesis of new carbon nanomaterials, including fullerenes and CNTs.

The radical injection PECVD (RI-PECVD) is used for synthesis of CNWs. [13)–15),19)–21),49),50)] This equipment consists of 2 plasma sources, which can independently control the generation of multiple radical species. This chapter describes the overview of RI-PECVD equipment and growth condition of CNWs.

Fig. 2.1.1 shows the schematic diagram of the RI-PECVD used for synthesis of CNWs. This equipment has two plasma sources, which are surface wave plasma (SWP) at the top and capacitively coupled plasma (CCP) at the bottom.

CCP was introduced CH_4 gas and very high-frequency (VHF, 100 MHz) power supplied to the upper electrode of the parallel-plate. SWP was introduced H_2 gas and microwave (2.45 GHz, 400 W) power supplied to the top chamber. Thus, this equipment can be controlled to generate methyl and hydrogen radicals independently.

The chamber was exhausted by a turbo molecular drug pump evacuated with a rotary pump. The background pressure was approximately 10^{-4} Pa. The pressure was

measured by a capacitance manometer.

The substrate was introduced from the load lock chamber, and placed at the lower electrode of the parallel-plate. The edge of substrate was fixed by a ring-shaped holder of the stage made of molybdenum using hex screw bolts.

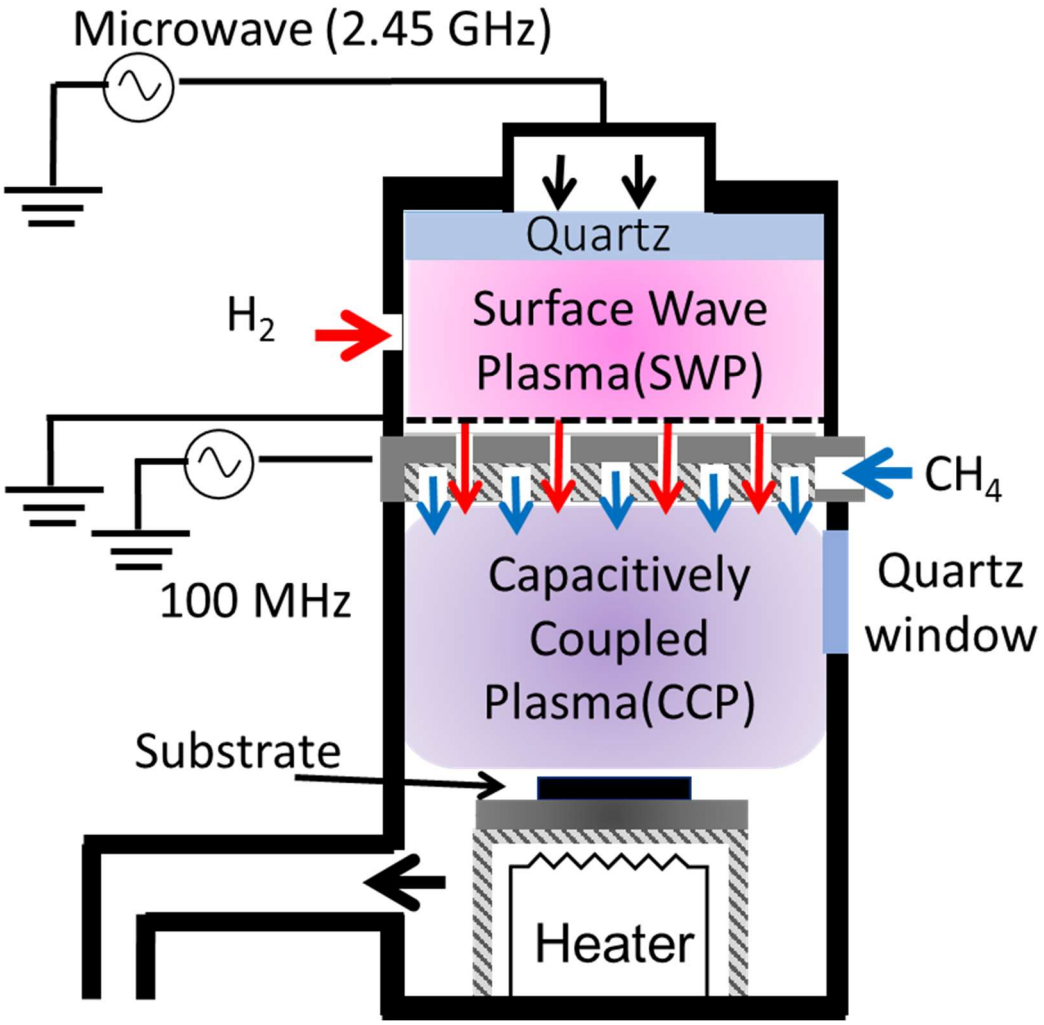

Fig. 2.1.1 A schematic representation of the RI-PECVD system

2.1.2 Optical Emission Spectrometry (OES)

Optical emission spectroscopy (OES) is performed by collecting light from the plasma with a lens connected to a fiber. In this research, optical emissions were measured by the spectrometer (Ocean optics, USB2000+) and the optical fiber for evaluation of plasma discharge through the quartz window equipped at the system viewing just beneath of the CCP electrode. The acquisition time was every 1 s.

2.1.3 Raman spectroscopy

Raman spectroscopy is widely used for analysis of the crystal structures. When monochromatic light with the frequency of ν0 is irradiated to a substance, the scattered light is observed and the most of scattered light is the light with the same frequency of ν0 (Rayleigh scattering), but also contains the light with the shifted frequency of ν0 ± νi (Raman scattering). Light with the frequency of ν0 - νi is called Stokes ray. Raman spectrum is plotted as the intensity of Stokes ray on the vertical axis and the frequency of νi on the horizontal axis. Since the frequency of νi corresponds to the molecular kinetic energy of a material, frequency of νi, peak intensity and full width half maximum of the intensity (FWHM) of Raman spectrum can be used for analysis of the molecular structure, chemical bonds, and crystallinity.

A Raman spectrum of CNWs mainly consists of G band (~1580 cm^{-1}), D band (~1360 cm^{-1}) and D' band (~1620 cm^{-1}). [51),52)] In the spectrum of CNWs, relative intensity of D and D' band to a G band is high (I_D/I_G > ~1) and FWHM of G band peak intensity ($FWHM_G$) is relatively broad compared to that of graphite.

In this study, Raman spectra of CNWs were acquired using Raman spectroscopy with an excitation power of 0.25 mW from a 532 nm laser (Renishaw inVia Raman).

2.1.4 Evaluation of wall-to-wall distance of CNWs

The wall-to-wall distances of CNWs is one of the important indicators in defining the structure of CNWs. [11),12)] The wall-to-wall distances of CNWs was calculated from a top image of scanning electron microscope (SEM) image.

The calculation method is shown in Fig. 2.1.2. ① At first, draw a straight line on the SEM image. ② Count the number of CNWs walls that cross this straight line. After that, the average wall spacing was calculated by dividing the length of the straight line by the number of walls of CNWs. A total of four straight lines were drawn vertically, horizontally, and diagonally so as to pass through the center of the image.

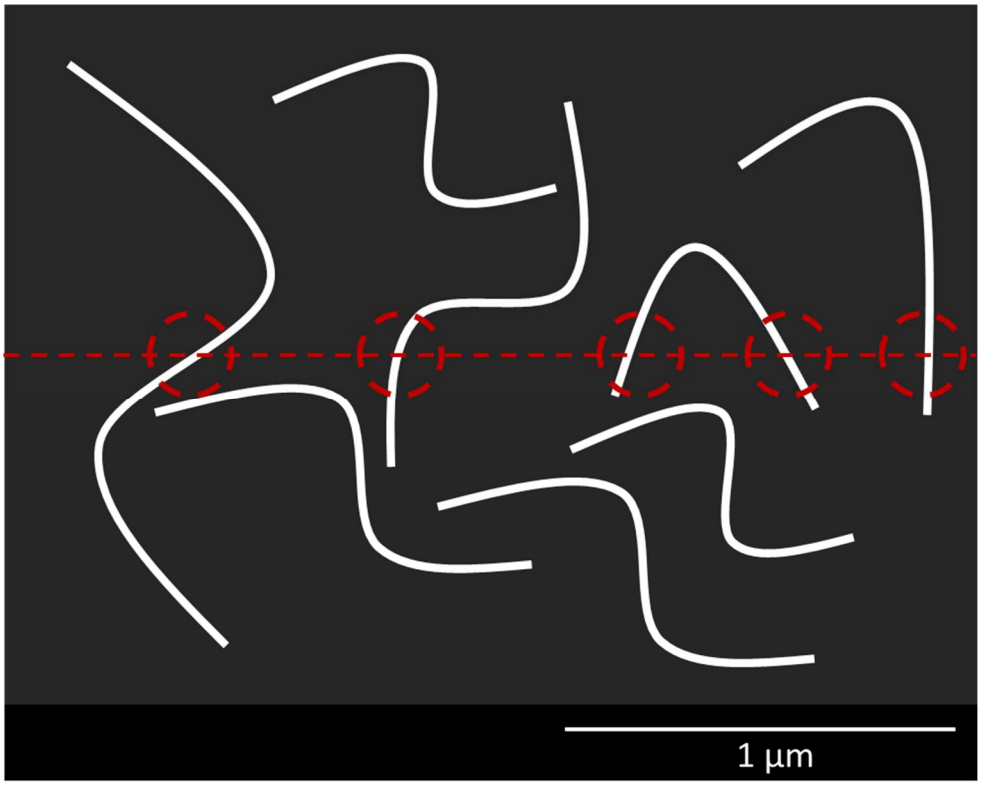

Ex.)

Straight line: 2.5 µm

Number of walls: 5

⇒Wall-to-wall distances: 2.5 µm / 5 = 500 nm

Fig. 2.1.2 The schematic diagram of the top image of CNWs and the evaluation method of wall-to-wall distances of CNWs

2.2 Methods of culture and evaluation of cells

2.2.1 Culturing Saos-2 cells

This section describes the cells used in the experiment and the culture method. Osteoblast-like cells (Saos-2) were used in this experiment. Saos-2 was incubated in DMEM+ (Dulbecco's modified Eagle's medium (DMEM; Sigma-Aldrich Co. Ltd., D5796-500ML) supplemented with 10% fetal bovine serum (Thermo Fisher Scientific, Inc., 10437-028), 100 units/ml penicillin, and 100 μg/ml streptomycin (Thermo Fisher Scientific, Inc., 15140-122)) in a humidified atmosphere of 5% CO_2/95% air at 37°C. Control and experimental cultures were kept in the same incubators.

2.2.2 Culturing cell on the CNWs scaffold

Cells on the CNWs scaffold were cultured by using a culture device originally designed and manufactured (NU-Rei Co., Ltd.) as shown in Fig. 2.2.1.

The CNWs is sandwiched between two acrylic plates and fixed with bolts. The upper acrylic plate had four circular holes with a diameter of about 1.128 cm, in which cells were cultured. The area is $\pi \times (1.128 / 2)^2 \approx 1$ cm^2, and the thickness of the upper acrylic plate is 1 cm, so the capacity of one well is 1 ml. In addition, a silicone sheet with a hole is sandwiched between the upper acrylic plate and CNWs at the same location as the culture chamber, and this silicone sheet prevents the culture medium from flowing out from the gap between the acrylic plate and CNWs. The copper wires for applying ES were taped to titanium substrate and it was confirmed electrical resistance value of this equipment was less than 1Ω. This device was used as a culture dish for CNWs scaffolds.

The wells were washed before seeding the cells. First, UV was irradiated for 15 minutes, and then 300 μl of Dulbecco's phosphate-buffered saline (PBS; Thermo Fisher Scientific, Inc., 14190-144) was added per well and stabilized for 15 minutes. After this stabilization, PBS was removed from the well and washed with PBS, and then 300 μl of DMEM+ was added and allowed to stand for 1 hour. After the 1-hour treatment, DMEM+ was removed and cells were seeded.

In addition, a 48-well plate (Costar® 3548, Corning) is generally used as a culture dish for comparison and it was prepared and cultured under the same conditions.

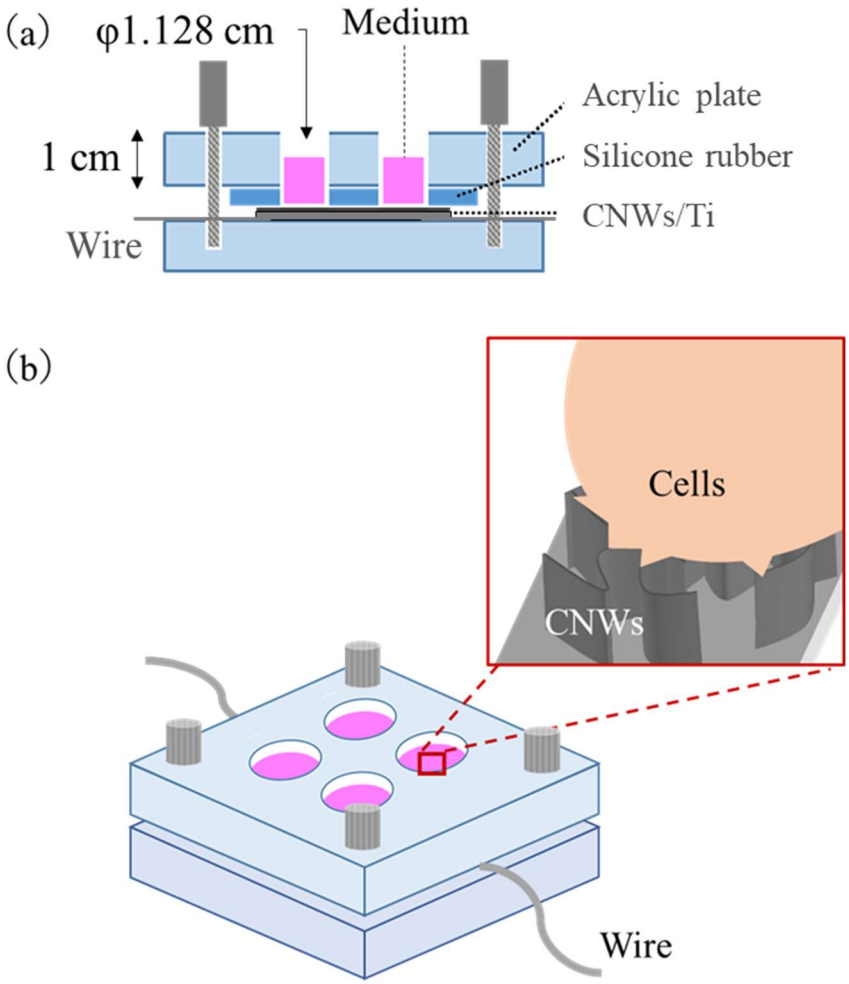

Fig. 2.2.1 (a) cross sectional view and (b) bird's-eye view of device culturing cells on CNWs

2.2.3 Culturing method with electrical stimulation on CNWs scaffold

Fig. 2.2.2 is a schematic diagram of the system constructed for culturing using application of ES in this study.

A function generator ((1) Tektronix, Inc., AFG3022B, (2) Kenwood Corporation, FG-281, (3) Toyo Technica Co., Ltd., BIOMATION 2416A) was used as the power source. The power sources are connected to CNWs scaffold via a 1-MΩ resistor.

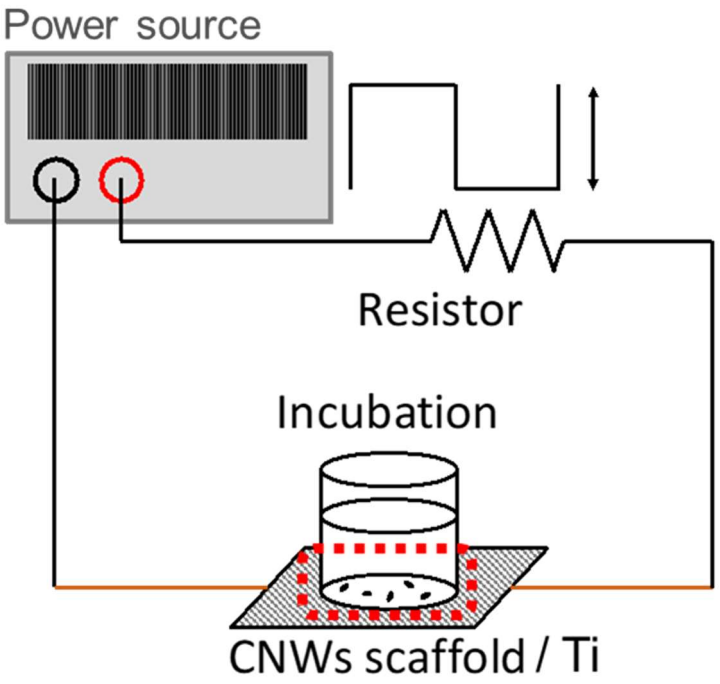

Fig. 2.2.2 Schematic diagram of electrical stimulation applied for culturing cells on CNWs scaffold.

2.3 Cell number measurement by colorimetric quantitative analysis (MTS test)

A method for measuring the number of cells is used by colorimetric quantitative analysis. In this study, the MTT method was used to measure the number of cells.

MTS (3- (4,5–dimethylthiazol–2-yl) -5- (3-carboxymethoxyphenyl) –2- (4-sulfophenyl) -2H-tetrazolium) is biologically reduced by cells and converted to a formazan. This conversion was carried out by nicotinamide adenine dinucleotide phosphatase hydrogen (NADPH) or nicotinamide adenine dinucleotide hydrogen (NADH) produced by metabolically active cellular dehydrogenases.[53] The amount of formazan product, expressed as absorbance at 490 nm, is proportional to the number of viable cells contained in the culture medium. The MTT-assay reagent [CellTiter 96® AQueous One Solution Cell Proliferation Assay [G3582] (Promega Corporation)] was used in this study.

After culturing cells, 300 μL of the MTT-assay reagent (CellTiter 96® AQueous One Solution Reagent) was added to each well, and the cells were cultured in an incubator at 37 °C in a 5% CO_2 atmosphere for 1 hour. The supernatant medium was then transferred to a 48-well plate and the absorbance of 490 nm was measured using a plate reader (BioTek Instruments, Inc., Synergy HTX Multi-Mode Reader). This absorbance value was calibrated to the number of cells using a disposable hemocytometer (4-chambers, [521-10] manufactured by Funakoshi Co., Ltd.).

2.4 The evaluation of the expression levels of mRNA

This section describes that the real-time polymerase chain reaction (real-time PCR) method used for measuring the expression level of intracellular messenger ribonucleic acid (mRNA).

PCR is a method of amplifying a target DNA region by a cycle reaction (double-strand dissociation→ annealing with primers→ extension reaction) of DNA as a template and complementary primers and thermostable DNA polymerase at both ends of the region to be amplified. After extracting mRNA from cells, complementary DNA (cDNA) was synthesized because of more stable than mRNA, and the target amount of mRNA was evaluated by this method with a reaction solution containing a fluorescent reagent.

At first, RNeasy Mini Kit (Qiagen, 74104) and Rnase-Free DNase set (Qiagen, Valencia, California) were used for mRNA purification. The amount and purity were measured using NanoDrop™ One (Thermo Fisher, ND-ONE-W).

The 260 nm peak intensity A_{260} measured by the Nanodrop is proportional to the mRNA concentration, and the 280 nm peak intensity A_{280} is proportional to the protein concentration. The theoretical value of A_{260} / A_{280} for 100% pure RNA was around 2.0. The A_{260} / A_{280} was experimentally confirmed to be proportional in a range from 1.97 to 2.05 under all conditions in this study.

Then, cDNA was synthesized from 1 μg of RNA using Omniscript^{TM} Reverse Transcriptase (QIAGEN, 205111). 9 μl reaction solution was prepared by mixing 3.4 μl of RNase Free water, 5.0 μl of 2 x KOD SYBER qPCR Mix (TOYOBO, QKD-201), 0.2 μl of 10 μM Forward primer and 0.2 μl of 10 μM Reverse primer. The primers shown in Table 2.4.1 were used as the primers. 9 μl of the mixed solution and 4-fold diluted cDNA solution in a 98-well plate and let stand at 98 °C for 2 minutes, then (1) double-stranded dissociation: 10 s at 98 °C, (2) annealing with primer: 10 s at 60 °C, (3) Stretching reaction: reaction at 68 °C for 10 seconds was performed for 40 cycles. These cycle reactions were performed using Light Cycler® 480 System II (Roche diagnostics). The expression levels of Runx2 and OC were evaluated by dividing by Ribosomal protein S18 (RPS18).

Table 2.4.1 Primer sequence

	Forward primer	Reverse primer
RPS18	5’ TTCGGAACTGAGGCC 3’	5' TTTCGCTCTGGTCCG 3'
Runx2	5’ AACCCACGAATGCACTATCCA 3’	5’ CGGACATACCGAGGGACATG 3’
OC	5’ TAGTGAAGAGACCCAGGCGC 3’	5’ CACAGTCCGGATTGAGCTCA 3’

2.5 Cell imaging using a fluorescence microscope and quantification of intracellular factors

In this section, the treatment of cells for observing cells with a fluorescence microscope is described.

2.5.1 Chemical fixation of cells

The chemical fixation of cells was carried out for observation of a scanning electron microscope (SEM) or when staining intracellular proteins or ions. This section describes the chemical fixation method for cells.

At the beginning of chemical fixation, the medium was removed, cells were washed, 300 μL/cm^2 of a PBS mixed with 4% paraformaldehyde / phosphate buffer (Wako Pure Chemical Industries, Ltd., 4% PFA: 4% Paraformaldehyde Phosphate Buffer Solution [163-20145]) was added, and stood for 30 minutes at room temperature.

Next, before observation by SEM, 4% PFA was removed, cells were washed with PBS, 70% of ethanol with pure water was added and it stood at room temperature for 10 minutes. Then, 70% of ethanol was removed and dried by replacement of 90%, 95%, and 99.5% of ethanol in order, each left to stand for 10 minutes.

2.5.2 Staining method mitochondria

To observe the shape of the cells with a fluorescence microscope, mitochondria in Saos-2 cells were stained with MitoTracker reagent (Thermo Fisher Scientific, Inc., MitoTracker® Red CMXRos [M7512]). The staining procedure is described below. 50 μg of MitoTracker, 96 μL of anhydrous dimethyl sulfoxide (Sigma-Aldrich Co. LLC, DMSO: Dimethyl sulfoxide [276855]) was added and stirred to a preservative solution of 1 mM MitoTracker. This preservative solution was stored in a −30 °C freezer (Biomedical Freezer [MDF-U539] manufactured by Panasonic Healthcare Co., Ltd.). The required amount of this 1 mM preservative solution was prepared by diluting it with a culture solution of 200 nM. The medium was removed from the incubator and it was washed with PBS once. Subsequently, a 200 nM staining solution was added to the incubator, and the cells were cultured in an incubator at 37 °C. in 5% CO_2 atmosphere for 30 minutes. Then, the staining solution was removed, DMEM+ was added, and fluorescence observation was performed using an optical microscope. A Texas Red filter (λex = 596 nm, λem = 615 nm) was used to observe with an upright microscope (ECLIPSE Ni, Nikon Corp.).

2.5.3 4',6-diamidino-2-phenylindole （DAPI）

4',6-diamidino-2-phenylindole (DAPI) is a fluorescent dye that strongly bind to DNA. DAPI is used as a reagent for staining cell nuclei in fluorescence microscopy. Also, in this study, DAPI (DOJINDO, 340-07971) was used to stain the cell nuclei.

2.5.4 Filamentous actin (F-actin)

Filamentous actin (F-actin) is intercellular protein and formed the cytoskeleton. F-actin were stained with phalloidin. A phalloidin is a kind of amanita-derived component also known as phallotoxin, bind to F actin and suppress actin depolymerization. In this study, Acti-stain^{TM} 488 phalloidin (CYT, PHDG1-A) was used.

Chapter 3 Effect of electrical stimulation on proliferation and bone formation by osteoblast-like cells cultured on CNWs scaffolds

3.1 Introduction

A number of reports of the combination of ES and carbon nanomaterials such as CNWs in cell culture applications have increased recently. Supronowicz et al. reported that the combination of ES at 10 Hz and a scaffold made of poly lactic acid and carbon nanotubes induced the proliferation of osteoblasts and their differentiation to form bone.[46] The CNW scaffolds electrical properties, such as high conductivity and morphologic properties, offer advantageously to control cell behaviors with ES. However, there is no report of the cell culture on CNW scaffolds in conjunction with ES.

This study conducted using microscopy and Alizarin red S (ARD SET) staining to evaluate the proliferation and bone formation of osteoblast-like cells (Saos-2) cultured on a CNW scaffold in conjunction with ES.

3.2 Experimental details

First, CNWs were synthesized using a radical injection plasma-enhanced chemical vapor deposition (RI-PECVD) system, as shown in Fig. 2.1.1. The flow rate of methane (CH_4) was 100 sccm, and that of hydrogen (H_2) was 50 sccm. The substrate temperature was 650°C, and the total pressure was 1 Pa. The distance between CCP electrodes was 30 mm. The power applied to the SWP and CCP sources was 400 W each. CNWs were synthesized on a Ti substrate, and the thickness of final CNWs was approximately 500 nm.

Fig. 3.2.1 (a) shows a top view of SEM image of CNWs. Two-dimensional carbon sheets were grown vertically on the substrate, forming a unique nanostructure similar to a maze.

Raman spectra of the CNW samples were acquired using the 532-nm line of a laser. As shown in the Raman spectrum in Fig. 3.2.1 (b), CNWs produced a strong peak at 1590 cm^{-1} (G-band), indicating the formation of a graphitized structure. Another peak was observed at 1350 cm^{-1}, which corresponded to the disorder-induced phonon mode (D-band).

Saos-2 cells were incubated in Dulbecco's modified Eagle's medium (DMEM) (Sigma, D5796) in a humidified atmosphere of 5% CO_2/95% air at 37°C, details were described in Chapter 2.2. A total of 3,000 cells were seeded in each well and incubated for 24 h, after which ES was initiated and continued during the culture period of 4 days. Direct current (DC) pulse power was supplied by function generators (Tektronix, Inc., AFG3022B). The generators provided ES via an alternating voltage of 226 mV with a square waveform at a frequency of 10 Hz.

Mitochondria within cells were stained and observed using the methods shown in Chapter 2.5.2.

Cell viability was evaluated after incubation for 4 days using the methods shown in Chapter 2.3.

Extracellular calcium levels were measured after 106 h of incubation with ES. The cells were then cultured for 10 days. Thereafter, the cells were rinsed twice with calcium- and magnesium-free PBS. The extracellular calcium concentration was determined using ARD SET (PG Research, Inc.) according to the manufacturer's instructions. The light absorbance of calcium-containing samples was determined

spectrophotometrically (575 nm) and normalized to that of a control sample.

(a)

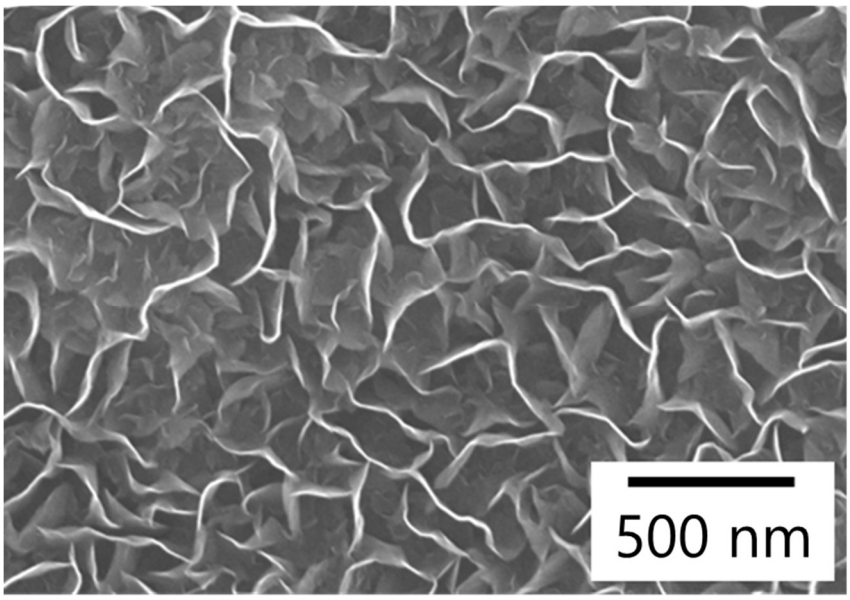

(b)

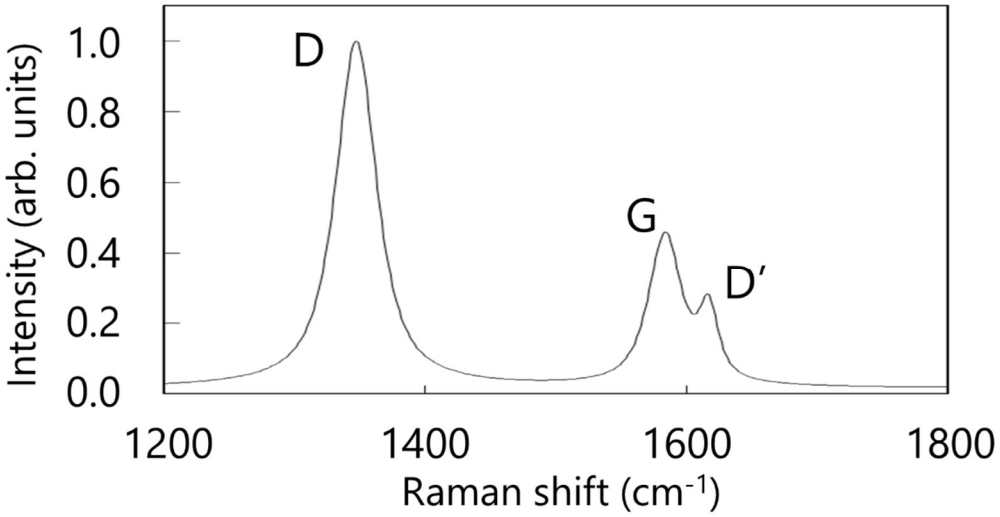

Fig. 3.2.1 Characterization of the CNW scaffold. (a) Top-view SEM image of CNWs synthesized using the RI-PECVD system. (b) Raman spectrum of CNWs.

3.3 Cell morphology on CNWs scaffold

Fig. 3.3.1 shows the top views of SEM images of cells on CNWs scaffold and on Si substrate. A Si substrate was prepared as a scaffold for smooth surfaces for evaluation the effect of the structure of CNWs on cell morphology. 24 h after seeding, the cells were chemically immobilized and sputtered with gold to prevent charging. The black part is the Saos-2 cells. It is found that the cells morphology is different between the Si substrate and CNWs scaffold as shown in Fig. 3. 3. 1 (a) and (d). Also, Fig. 3.3.1 (e) and (f) indicate that the edges of the cells extend along the shape of the tip of the wall of the CNWs and adhere in a mesh pattern under the influence of the structure of the CNWs.

Fig. 3.3.2 shows the cross-section view of SEM image of the cells on the CNWs scaffold. In this image, a stack of Si substrate, CNWs and cells is recognized and the cells were attached to a part with a few nanometers of the top of the CNWs.

Cells were uniquely adhered on the CNWs and changed morphologically at peculiar to the CNWs scaffolds. The cell shape is influenced by the structure of the CNWs, owing to the edge of the CNWs that are only the adhesive surface.

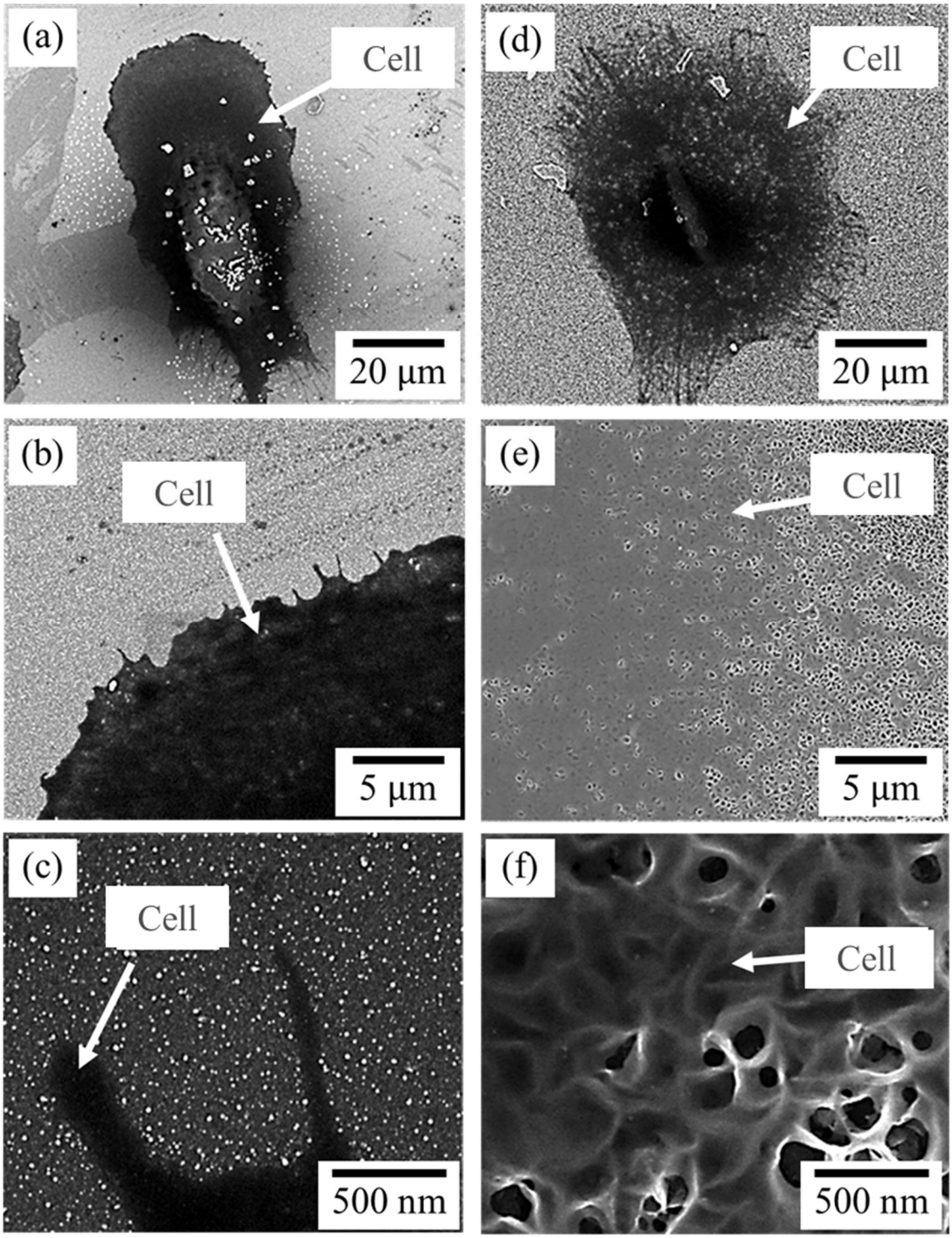

Fig. 3. 3. 1 The top views of the SEM image of the Saos-2 cells cultured on Si substrate((a), (b), (c)) and the CNWs scaffold((d), (e), (f))

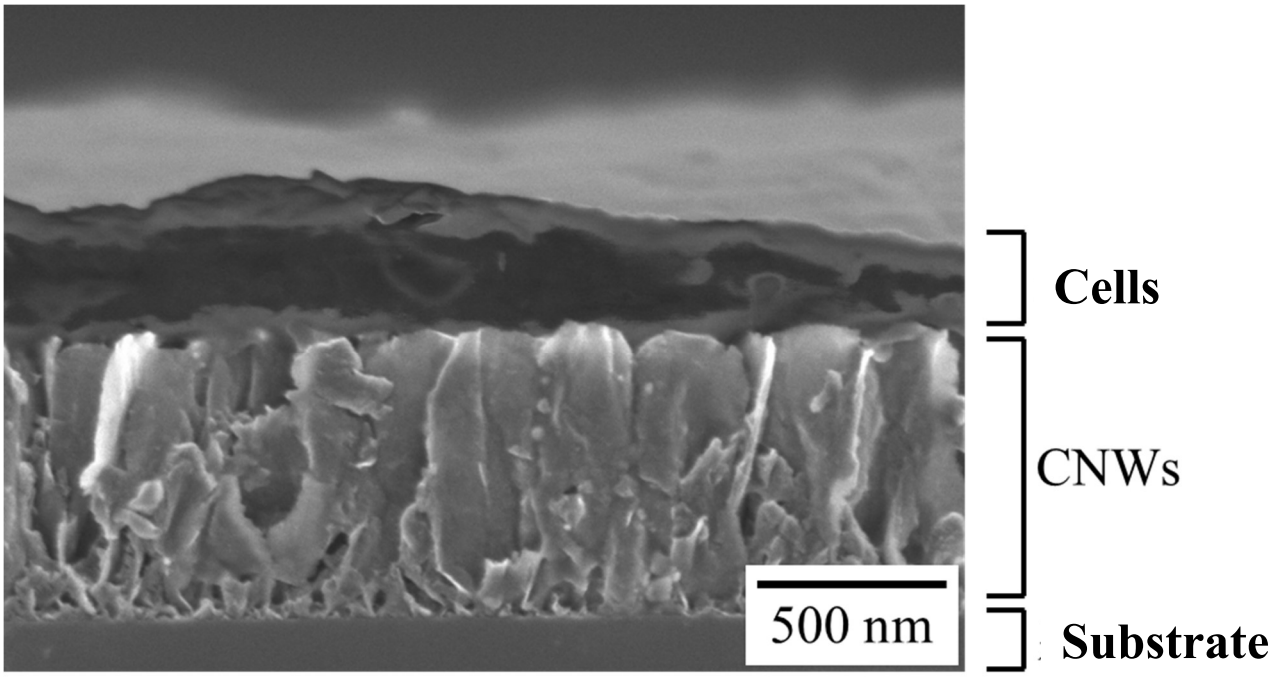

Fig. 3. 3. 2The cross view of the SEM image of Saos-2 cells cultured on CNWs

3.4 Proliferation and bone formation of cells cultured on CNWs scaffold

The morphology of cells incubated for 4 days in 24-well plates was observed by differential interference contrast microscopy (Fig. 3.5.1 [a]) and fluorescent staining of mitochondria (Fig. 3.5.1 [b, c]). Micrographs of cells on the CNW scaffold without and with ES are shown in Fig. 3.5.1 (d) and (e), respectively. As previously described, the ES conditions were 10-Hz squared 226-mV electrical current pulses. On the 24-well plate, the Saos-2 cells exhibited a normal appearance, adhering independently at a distance, as shown in Fig. 3.5.1 (c). Interestingly, on CNW scaffold, adhering cells formed an agglomeration, called a nodule, as indicated by arrows in Fig. 3.5.1 (d, e). Cells cultured with ES formed larger nodules than cells cultured without ES, indicating that ES of Saos-2 cells on a CNW scaffold promotes nodule formation and differentiation leading to bone formation.

Fig. 3.5.2 (a) shows a number of cells incubated in the dish (46,873 ± 1,617) (mean ± standard error of the mean); a number of cells on the CNW scaffold without ES (20,377 ± 3,463); and a number of cells on the CNW scaffold with ES (32,032 ± 3,683) after 4 days of incubation. There was a significant difference between the number of cells in the 24-well plate and the number on the CNW scaffold without ES ($p<0.0005$) and between the number of cells in the 24-well plate and the number on the CNW scaffold with ES ($p<0.05$). ES applied for 4 days promoted a significant increase ($p<0.05$) in the number of cells on the CNW scaffold without ES. ES induced a 57% increase in the number of Saos-2 cells on the CNW scaffold.

Bone formation was assessed by measuring levels of extracellular calcium as an indicator. After 10 days, cells were stained with ARD SET, and the measured absorbance was normalized to that of the control. Fig. 3.5.2 (b) shows the normalized absorbance of cells incubated on a 24-well plate, a CNW scaffold without ES, and a CNW scaffold with ES. The absorbance of the cells incubated on the dish (100 ± 7.8%) was greater ($p<0.18$) than that of cells incubated on the CNW scaffold without ES (69 ± 18.4%). The absorbance of cells incubated on the CNW scaffold with ES by 10-Hz pulses for 10 days (54 ± 9.3%) was significantly lower ($p<0.01$), indicating that ES of cells on the CNW scaffold suppressed bone formation, as evidenced by the low level of extracellular calcium.

As shown in Fig. 3.5.2, the proliferation of cells cultured on the CNW scaffold increased in response to ES. In a previous study, Nomura et al. investigated the effect of ES frequency on the behavior of cells using an alkaline comet assay method over a frequency range of 0 to 10^5 Hz. Their results suggested that stimulation at a frequency of 10 Hz affected the cell membranes.[54] Dijak et al. reported aggregation of cells in a culture

dish following application of a DC electrical field.[55] In this case, ES could have affected the cell membrane to induce proliferation of cells on the CNW scaffold. The data thus also indicate that application of an electrical field affects cell proliferation.

Although proliferation and nodule formation were promoted in the case of cells cultured on a CNW scaffold with ES, bone formation was suppressed, as evidenced by the decrease in extracellular calcium concentration (Fig. 3.5.2(b)). In general, osteoblast agglomeration promotes the formation of bone or calcified nodules.[56] In contrast to these general phenomena, however, these experimental results are quite unique, as shown in Fig. 3.5.1 and Fig. 3.5.2. For example, although Saos-2 cells aggregated, the formation of calcified nodules was suppressed. The morphology of cells adhering to the CNW top edges changed compared with cells growing on the flat substrate.[48] It is possible that the adherence of the Saos-2 cells on the CNWs was weakened by their dispersal due to the wall structure and that the weak adherence in conjunction with ES promoted proliferation and nodule formation but suppressed calcification.

Therefore, controlling the synergistic effects associated with ES and the morphology of the CNWs is crucial for controlling cell proliferation and calcification. In general, cells cannot proliferate and simultaneously form bone. Weinstein et al. reported that a cycle of bone formation was necessary to control for increase in strength of promoted bones.[57] Although there are a number of methods for stimulating bone formation, a method for regulation or suppression of bone formation is limited. Thus, the technology of suppression of bone formation is an essential requirement for regenerative medicine. The results demonstrate that the method described is an effective means of multiplication of cell population of osteoblasts while suppressing bone formation. This technique provides methods to culture bone marrow stem cells without differentiation of bone formation.

3.5 Conclusion of this chapter

CNW scaffolds were synthesized using a RI-PECVD system. Saos-2 cells were cultured on the resulting CNW scaffold with ES pulses at a frequency of 10 Hz. When the cells were incubated on the CNW scaffold, ES promoted proliferation but bone formation and the formation of calcified nodules were suppressed in contrast to the case without ES. These results demonstrate the utility of cell culture methods using CNWs with ES to control osteoblast proliferation and bone formation for use in regenerative medicine.

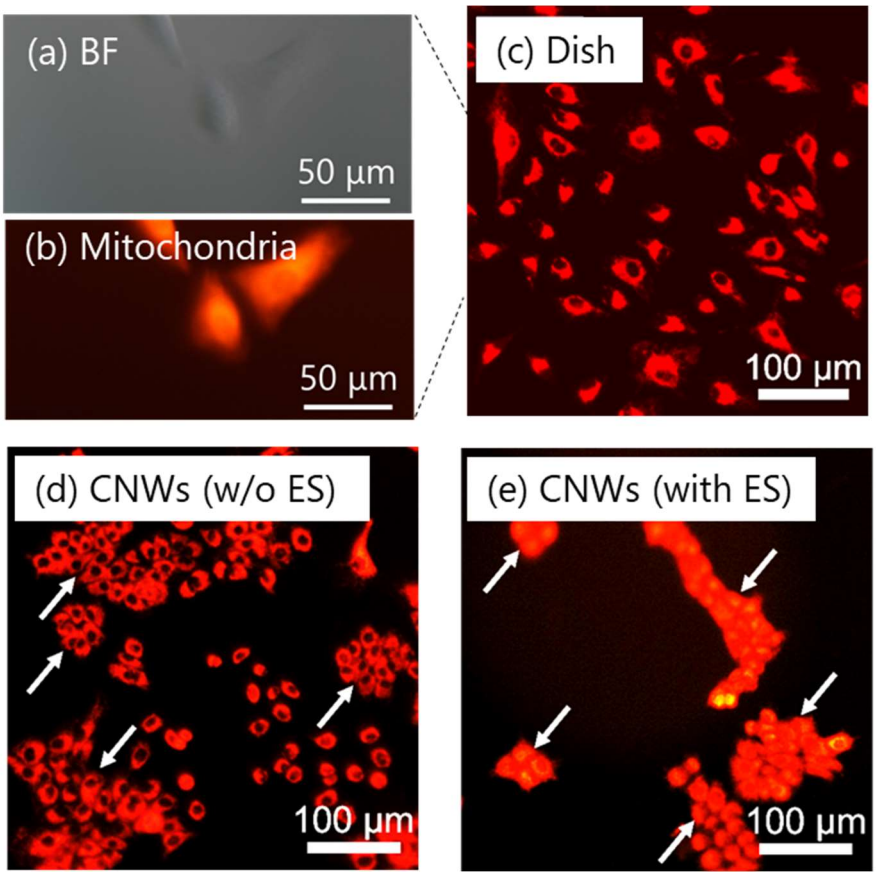

Fig. 3.5.1 (a) Bright field (BF) image of Saos-2 cells on a culture dish; fluorescence microscopy images of cells stained with Mito-tracker reagent (b), (c) on the dish, (d) on the CNW scaffold, and (e) on the CNW scaffold with ES.

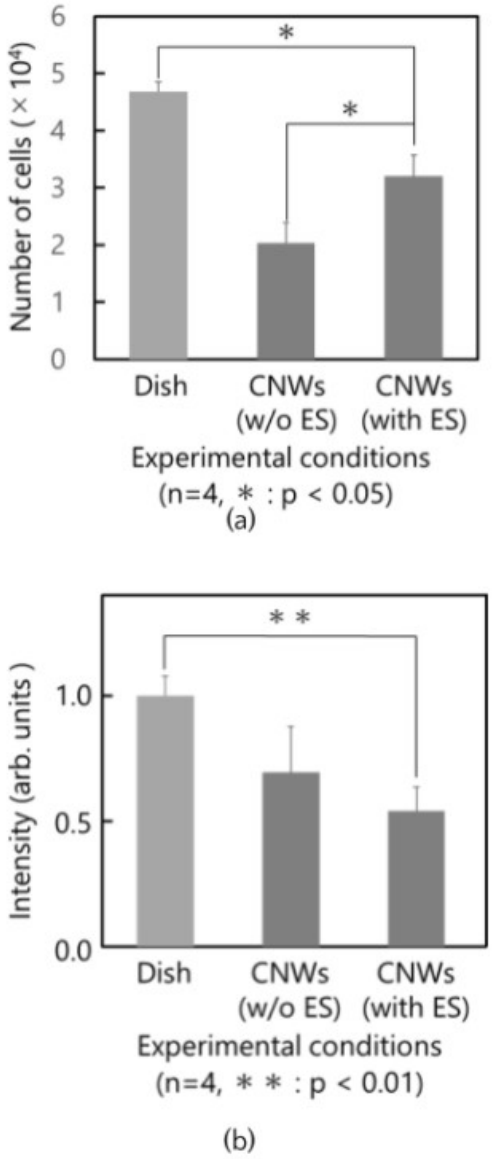

Fig. 3.5.2 (a) Number of cells as determined using the MTS assay after incubation for 4 days on (i) culture dish, (ii) CNW scaffold without ES, and (iii) CNW scaffold with ES. (b) Absorbance intensity of cultures stained with Alizarin red S after 10 days of culture on (i) a 24-well plate, (ii) a CNW scaffold without ES, and (iii) a CNW scaffold with ES.

Chapter 4 Gene expression of osteoblast-like cells incubated with electrical stimulation on carbon-nanowall scaffolds with different wall-to-wall distances

4.1 Introduction

CNWs are useful as a scaffold for culturing osteoblasts as shown in Chapter 3. Scaffolds aid cell proliferation, differentiation, and morphological control. There is no report about the effect of CNWs and the ES on the differentiation of osteoblasts.

In this study, the author investigated the effect of wall-to-wall distance in CNW scaffolds of different densities together with ES on the proliferation and differentiation of osteoblast-like cells (Saos-2). Cell viability was measured by the MTS colorimetric proliferation assay and real-time PCR was used to evaluate gene expression of the proliferating and differentiating osteogenic cells under these various conditions.

4.2 Experimental details

The scaffolds were prepared using in-house-deposited nanostructured carbon. CNWs were synthesized by the radical injection plasma-enhanced chemical vapor deposition (RI-PECVD) system, as shown in Fig. 2.1. The flow rates of methane (CH_4) and hydrogen (H_2) were100 sccm and 50 sccm, respectively. The substrate temperature was 650°C, and the total pressure was either 1 Pa or 3 Pa. The distance between the CCP electrodes was 30 mm. The power applied to the SWP source was 400 W and 200 W to the CCP source. CNWs were synthesized on a Ti substrate and the final CNWs were approximately 500 nm thick.

Fig. 4.2.1 shows a top view of SEM images of CNWs synthesized at (a) 1 Pa and (b) 3 Pa. Two-dimensional carbon sheets grew vertically on the substrate, forming unique nanostructures. Raman spectra of these CNW samples were measured using 532 nm laser irradiation. The peak at 1590 cm^{-1} (G-band) (Fig. 1 (c)) indicates the formation of a graphitized structure, and the peak at 1350 cm^{-1} corresponds to the disorder-induced phonon mode (D-band). The I_D/I_G ratio was around 2, as shown in
Table **4.2.1**. The CNW densities were expressed using the average wall-to-wall distances of 132 and 220 nm for samples synthesized at 1 Pa and 3 Pa, respectively, as shown in
Table **4.2.1**.

Saos-2 cells were incubated in Dulbecco's modified Eagle's medium (DMEM) (Sigma, D5796) in a humidified atmosphere of 5% CO_2/95% air at 37°C, details were described in Chapter 2. A 48-well cell culture cluster (Corning, 3548) was used as a control. Before cell culture, all components were washed with pure water and sterilized by exposure to ultraviolet light for 20 min. The wells were filled with 300 μl phosphate-buffered saline (PBS; Gibco Life Technologies) for 20 min, then the PBS was replaced with fresh PBS for 15 min. Finally, each well was filled with 300 μl DMEM supplemented with 10% fetal bovine serum (Life Technologies, 10437-028), 100 units/ml penicillin, and 100 μg/ml streptomycin (Life Technologies, 15140-122) and left for 1 h at room temperature. A total of 3,000 cells were seeded in each well and incubated for 24 h. ES was initiated after 1 day and continued during the 4 days culture period. The terminals of the CNW-deposited Ti substrate were connected via a 1-MΩ resistor to a direct current (DC) pulse power supply operated at 226 nA and a frequency of 10 Hz using a square waveform function generator (Tektronix, Inc., AFG3022B). The electrical resistance of the Ti substrate was <1 Ω.

Cell viability was evaluated after 4 days' incubation. The measurement method of cell viability was described in Chapter 2.3.

Mitochondria within the cells were observed by the method shown in Fig. 2.5.2, after 4 days' incubation.

Real-time PCR as described in Chapter 2.4 was used to detect mRNAs encoding Runt-related transcription factor 2 (Runx2) and osteocalcin (OC) after 10 days' incubation. Cells were seeded at around 1×10^5/well.

The morphological features of the cells were observed after incubation for 1 and 2 days. The cells were fixed by the method as shown in Fig. 2.5.1. Actin cytoskeleton was stained with 100 nM Acti-stain™ 488 phalloidin and nuclei were stained with 200 nM DAPI as shown in Figs. 2.5.3 and 2.5.4.

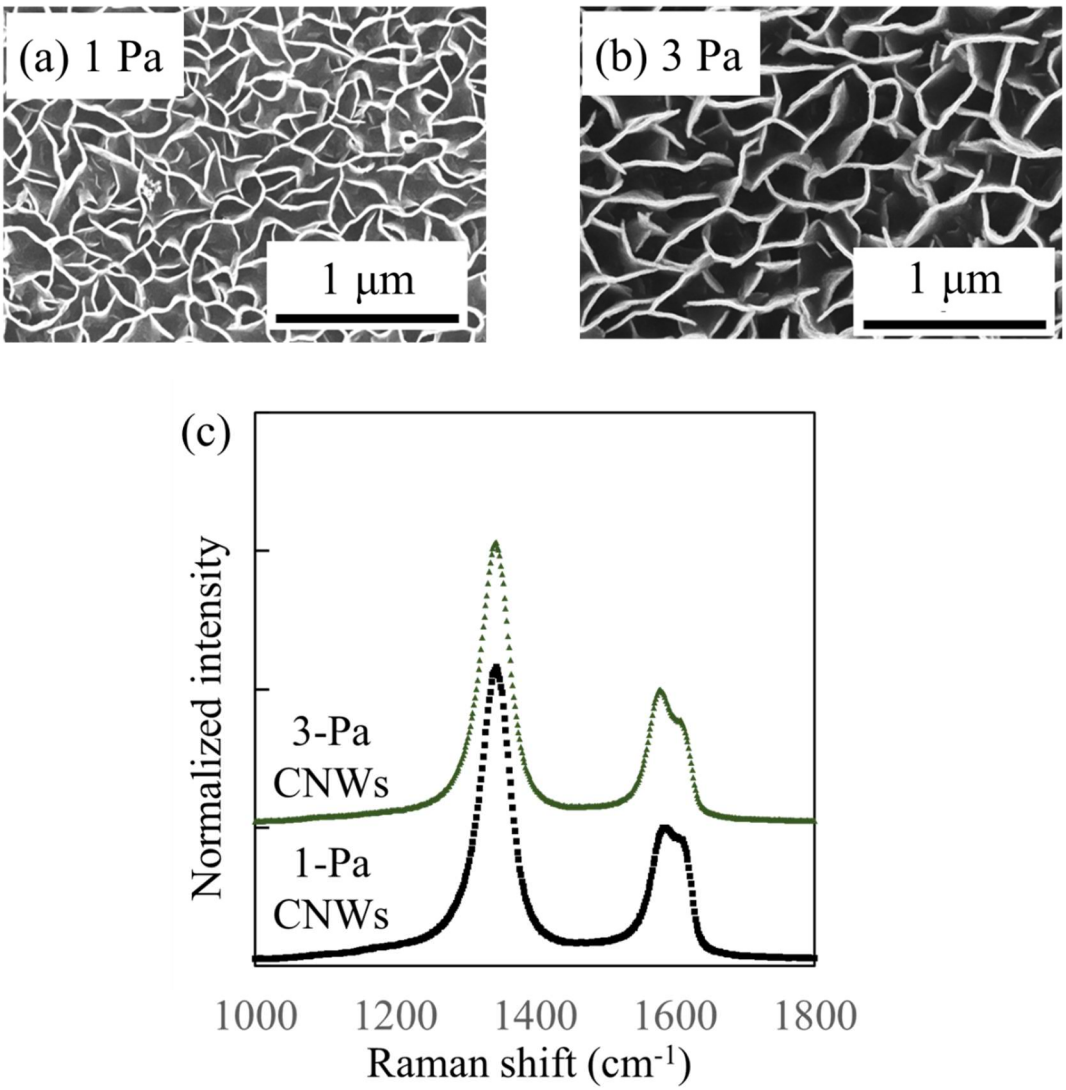

Fig. 4.2.1 Characterization of CNW scaffolds. Top views of SEM images of CNWs synthetized by RI-PECVD at (a) 1 Pa and (b) 3 Pa. (c) Raman spectra of the CNWs. Reprinted with permission from T. Ichikawa et al., ACS Appl. Bio Mater. 2, 7, pp. 2698–2702 (2019). Copyright 2019 American Chemical Society.

Table 4.2.1 Average wall-to-wall distances and I_D/I_G of CNWs synthetized by RI-PECVD at 1 Pa and 3 Pa.

	1-Pa CNWs	3-Pa CNWs
Average wall-to-wall distances (nm)	132	220
I_D/I_G	2.2	2.1

4.3 Results

Fig. 4.4.1 shows the number of cells after 4 days' incubation under various conditions. The largest number of cells grew on the polystyrene (PS) surface. The number of cells on the 1-Pa CNW scaffold was similar to that on the 3-Pa CNW scaffold in the absence of PS. In contrast, ES resulted in a significant difference in the number of cells on the 1-Pa and 3-Pa CNW scaffolds ($p<0.05$), and between the 3-Pa CNW scaffold without ES and with ES ($p<0.05$). ES increased the proliferation of Saos-2 cells by 58% on the 3-Pa CNW scaffold.

Micrographs of cells incubated for 4 days on the CNW scaffolds with and without ES (10-Hz square 226-mV electrical current pulses) following fluorescent staining of the mitochondria are shown in Fig. 4.4.12. The cells on the 1-Pa CNW and 3-Pa CNW scaffolds with ES were round, similar to cells detached from the bottom of the culture dish. This cell differentiation may be initiated by the expression of Runx2 and OC and thus the expression levels of these genes were evaluated by real-time PCR measurements.

Fig. 4.4.3(a) shows the relative expression levels of Runx2/RPS18 after incubating the cells under the various conditions for 10 days. The normalized expression in cells grown on PS, 1-Pa CNWs without ES, 1-Pa CNWs with ES, 3-Pa CNWs without ES and 3-Pa CNWs with ES were 1.0, 7.4, 2.8, 13.3 and 1.8, respectively, and these differences were significant for all conditions ($p<0.05$). Similarly, Fig. 4.4.3 (b) shows the relative expression levels of OC/RPS18 after incubation for 10 days. The normalized levels of cells grown on PS, 1-Pa CNWs without ES, 1-Pa CNWs with ES, 3-Pa CNWs without ES and 3-Pa CNWs with ES were 1.0, 6.9, 2.8, 13.7 and 1.5, respectively, and these differences were significant for all conditions ($p<0.05$) except for expression in cells grown on 1-Pa CNWs with ES and on 3-Pa CNWs with ES ($p=0.07$). The CNW scaffolds with wider wall-to-wall distances enhanced the differentiation of Soas-2 cells and ES suppressed differentiation.

Fig. 4.4.4 (a) shows fluorescence microscope images of cell nuclei and F actin in Saos-2 cells grown on (i) PS, (ii) 1-Pa-CNWs and (iii) 3-Pa-CNWs for 1 day. Actin filaments on the cell edge were affected by the wall-to-wall CNW distances. Fig. 4.4.4 (b) shows the average observed area of one Saos-2 cell after incubation for 1 day under the various conditions. The area of a cell incubated on PS was different from the area of

a cell incubated on 1-Pa CNW ($p<0.005$). Cells incubated on PS has significantly smaller areas compared with cells incubated on 3-Pa CNW ($p=0.066$). Fig. 4.4.4 (c) shows fluorescence microscope images of cell nuclei and F actin in Saos-2 cells grown for 2 days on (i) PS, (ii) 1-Pa CNW scaffold without ES, (iii) 1-Pa CNW scaffold with ES, (iv) 3-Pa CNW scaffold without ES and (v) 3-Pa CNW scaffold with ES. Cells grown with ES on 1-Pa and 3-Pa CNWs were round, as shown in Fig. 4.4.4 (d). Overall, ES affected cell morphology and actin filament formation. Cells generally adhere on scaffolds through actin polymerization. Thus, the rounded shapes may originate from modifications in actin polymerization due to the initiation of cell differentiation. This study proposes that the primary mechanism of adhesion is that actin polymerization suppressed the gene expression of Runx-2 and OC and promoted cell growth on CNW scaffolds.

The differentiation of Saos-2 cells incubated with 1-Pa CNW or 3-Pa CNW scaffolds was investigated using real-time PCR to quantify the gene expression of Runx2 and OC. The results of actin observations showed that the cells adhered weakly to the CNW scaffolds, suppressing actin polymerization. Sen et al. reported that human mesenchymal stem cell differentiation was promoted by chemically inhibiting actin polymerization.[58] This suggests that cell differentiation can be promoted by inhibiting the formation of actin filaments, thereby providing a novel method for regulating cell proliferation and differentiation without chemical stimulation.

4.4 Conclusion of this chapter

Saos-2 cells were incubated on CNW scaffolds with different wall-to-wall distances synthesized using a RI-PECVD system and ES pulses with a frequency of 10 Hz were applied during incubation. The expression of Runx-2 and OC was suppressed during ES application and cell proliferation was enhanced by scaffolds with narrower wall-to-wall distances. This demonstration of osteoblast proliferation and cell differentiation may have application as a cell culture method for regenerative medicine.

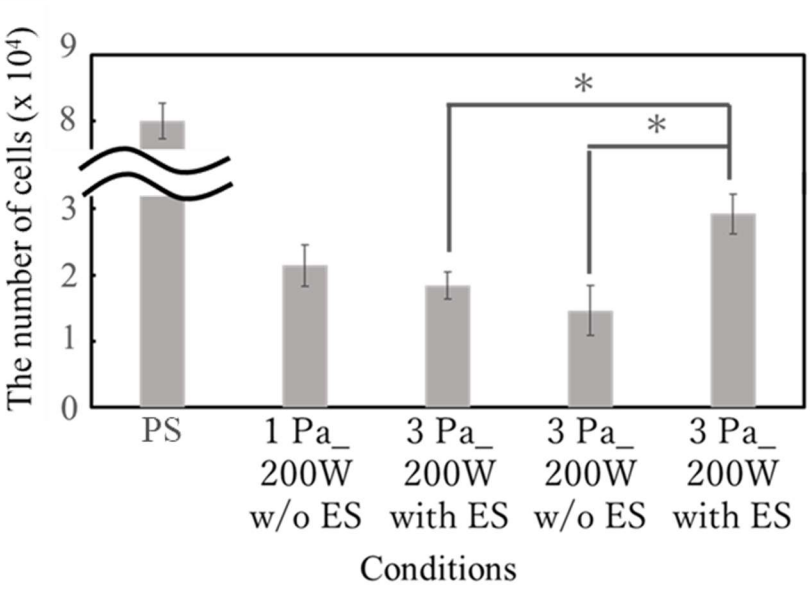

Fig. 4.4.1 Number of cells determined using the MTS assay after incubation for 4 days on PS,1-Pa CNW scaffold without ES, 1-Pa CNW scaffold with ES, 3-Pa CNW scaffold without ES, 3-Pa CNW scaffold with ES (N=3, * ：$p<0.05$). Reprinted with permission from T. Ichikawa et al., ACS Appl. Bio Mater. 2, 7, pp. 2698–2702 (2019). Copyright 2019 American Chemical Society.

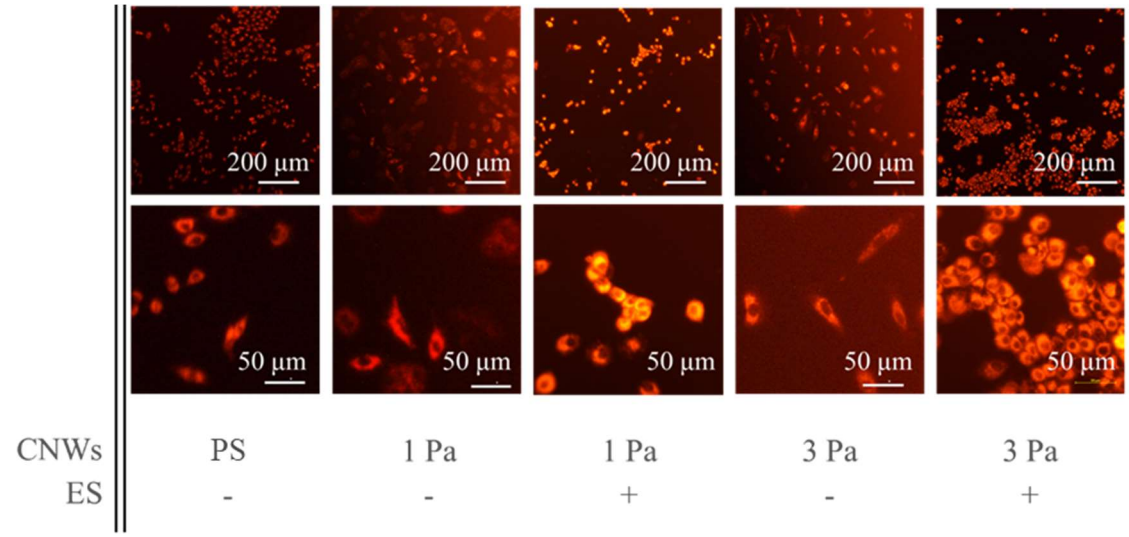

Fig. 4.4.2 Fluorescence microscopy images of cells stained with Mitotracker reagent after incubation for 4 days on PS, 1-Pa CNW scaffold without ES, 1-Pa CNWs scaffold with ES, 3-Pa CNW scaffold without ES, 3-Pa CNW scaffold with ES. Reprinted with permission from T. Ichikawa et al., ACS Appl. Bio Mater. 2, 7, pp. 2698–2702 (2019). Copyright 2019 American Chemical Society.

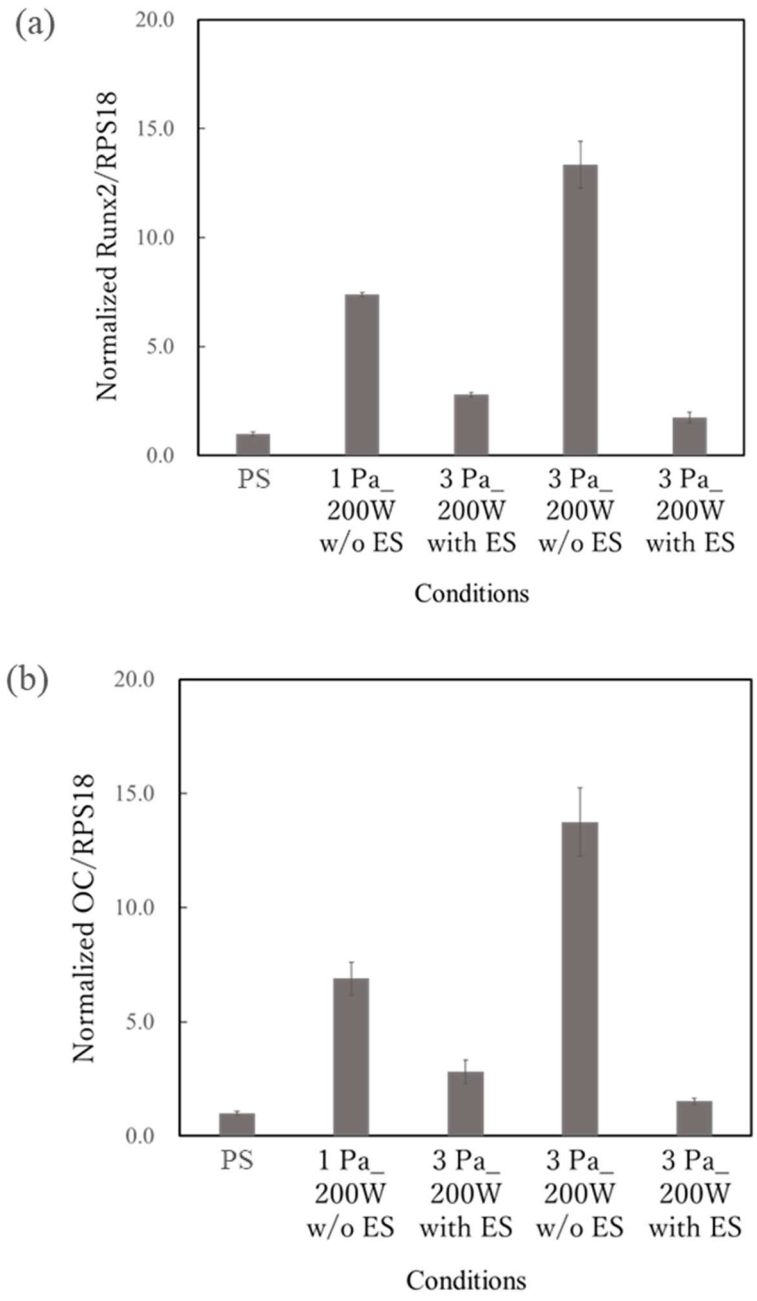

Fig. 4.4.3 Relative levels of bone marker expression determined using real-time PCR after incubation for 10 days. (a) Runx2 and (b) OC following culture on (i) PS, (ii) 1-Pa CNW scaffold without ES, (iii) 1-Pa CNW scaffold with ES, (iv) 3-Pa CNW scaffold without ES, (v) 3-Pa CNW scaffold with ES. Reprinted with permission from T. Ichikawa et al., ACS Appl. Bio Mater. 2, 7, pp. 2698–2702 (2019). Copyright 2019 American Chemical Society.

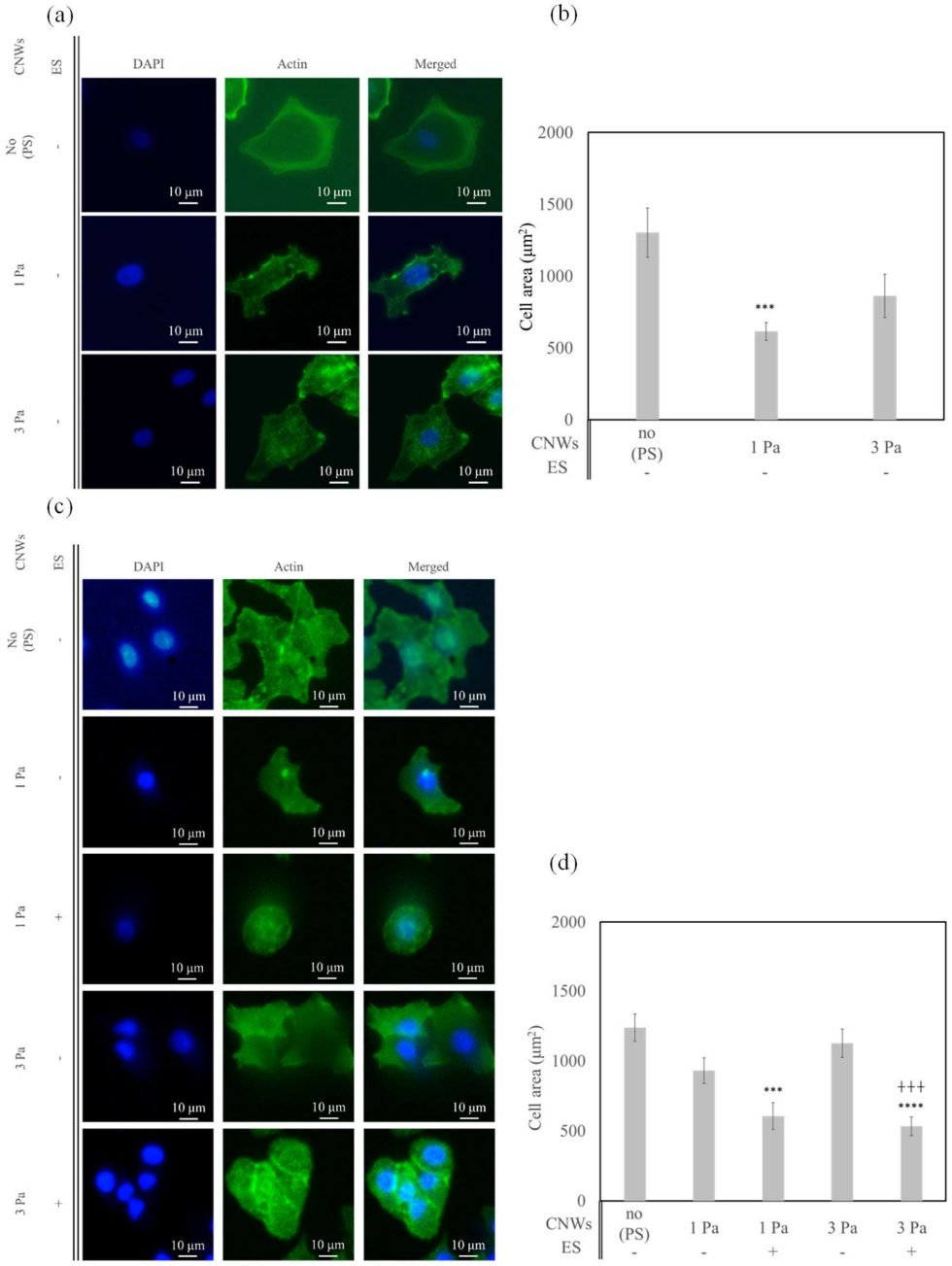

Fig. 4.4.4 Fluorescence microscope images of cells stained with DAPI and Acti-stain 488 phalloidin solution after incubation (a) for 1 day on PS, 1-Pa CNW, and 3-Pa CNW and (c) for 2 days on PS, 1-Pa CNW scaffold without ES, 1-Pa CNW scaffold with ES, 3-Pa CNW scaffold without ES, and 3-Pa CNW scaffold with ES. (b), (d) show the area per cell calculated from the fluorescence microscope images. (n=7, ***: $p<0.005$ compared to the area of cells grown on PS and +++:$p<0.005$ compared to the area of cells grown on 3-Pa CNW scaffold without ES). Reprinted with permission from T. Ichikawa et al., ACS Appl. Bio Mater. 2, 7, pp. 2698–2702 (2019). Copyright 2019 American Chemical Society.

Chapter 5 Synthesis of sparsely isolated carbon nanowalls by high-voltage nanosecond pulses application in CH_4/H_2 plasma enhanced chemical vapor deposition

5.1 Introduction

CNW structures are common to interconnect walls each other. A sparse CNW film has not synthesized yet. However, sparsely isolated CNW structure with wider averaged wall-to-wall distances of CNWs than 1 μm requires for the application of cell culturing scaffold as shown in Chapter 4.

The CNWs films are typically synthesized by plasma-enhanced chemical vapor deposition (PECVD) system. The averaged wall-to-wall distances of CNWs were controlled by changing conditions of the plasma discharges.[11] The growth mechanism of CNWs is considered to be comprised of two stages of nucleation of adsorbed carbon atom and a wall-like growth of the graphene sheets.[13),50),59)–62] Kondo et al. proposed the growth model that CNWs were nucleated in the early growth period and growth starts only under the specific conditions in terms of a balance between ion and radical fluxes.[50] The balance was experimentally clarified to be 200-eV argon ion (Ar^+) irradiation with ion fluxes ranged from 3.3 to 3.8 μA/cm^2 and radical density of the order of 10^{11} cm^{-3} of CF_3 and H.[13] The ion bombardment modifies the adsorption mechanism on a surface from physical sorption to the chemical sorption, while the radical can diffuse along the surface and can be adsorbed on sharp edges of nucleated flake-like graphene sheets.[59] Thus, this study assumes that the averaged wall-to-wall distance of the CNWs films is certainly determined by influxes of charged and neutral particle toward the grown surface. Furthermore, this study anticipates that the high-voltage nanosecond pulses can modify the ion fluxes. Pustylnik et al. ensured that the high-voltage nanosecond pulses within 20 ns swept away plasma electrons and flash-like excitation was triggered by acceleration of in electric fields of residual immobile bulk ions.[62] To apply this for modifying the fluxes of charged and neutral particles, the ion bombardments may be enhanced, when the pulse turns on, and the neutral radicals may be grown on the CNWs, when the pulse turns off.

This study has first attempted to use the high-voltage nanosecond pulses in the CNWs synthesis. Controlling of the averaged wall-to-wall distances of CNWs films in the RI-PECVD system has been achieved by alternation of the input voltage from 90 to

150 V to change electrostatic powers of the nanosecond pulses. Higher voltages provided wider wall-to-wall distances in average. Details of time dependence of the growth of CNWs were clarified the impact of high voltage nanosecond pulse application to the nucleation mechanism. Effects of the high-voltage nanosecond pulse applications on wall density in CNW films are discussed by building of a CNWs growth model.

5.2 Experimental details

The CNWs films were synthesized by the RI-PECVD system, as shown in Fig. 5.2.1. Low-pressure weakly ionized plasma was stationary generated by two tandem sources. A SWP source and a CCP are connected by a showerhead-type CCP electrode. 400 W of SWP and 400 W of CCP were applied. The distance between CCP electrodes and substrate was 30 mm. CH_4 with a flow rate of 100 sccm and that of H_2 of 50 sccm were introduced into the chamber and kept a total pressure of 1 Pa. The substrate temperature was maintained at 650°C during the deposition.

The substrate holder with an area of 32 cm^2 was electrically connected with the inductive energy storage (IES) circuit, as shown in Fig. 5.2.1. To shape high-voltage nanosecond pulses with high through rate, the holder was electrically cramped by a ballast resistor of 10 kΩ and a rectifier diode. The IES circuit was operated by input of DC voltage V_{in} and stored electrostatic energy in the storage capacitor, C_s.[62)–64)] The stored energy ($C_s \times V_{in}$) was switched by the static induction thyristor that was controlled by the driving circuit. The V_{in} was changed at 0, 90, 120, and 150 V for controlling the stored electrostatic energy. The pulse frequency of the IES circuit operation was 50k pulses per a second (pps), i.e., every 20 μs. Widths of each pulse were regulated automatically the IES circuit. DC current, I_{in}, for the IES input power supply was remained a constant of 0.5 A. The waveforms of the output voltage, V_{out}, and current, I_{out}, at the IES input voltages are recorded by using oscilloscope (Gwinstek GDS-3504), high-voltage probe (Tektronix P-6015A), and current probe (Pearson Electronics, Inc. Current monitor 2879), as typically shown in Fig. 5.2.2. The peak-to-peak voltage V_{peak} and the average voltage V_{av} were unchanged. Only the peak-to-peak current I_{peak} increased when the V_{in} was changed. It is noted that the IES power, P, was increased with increasing the IES input voltage, V_{in}. Peak-to-peak values for the waveforms were measured. The obtained parameters are summarized in Table 5.2.1.

Substrate was a Si (100) wafer with a size of 2 × 2 cm^2. After cleaning, the wafer was placed on the stage holder made of molybdenum. Deposition time was set for 290 s and the CNWs film thickness was approximately 500 nm.

The CNWs films were evaluated by SEM (Hitachi-high technologies, SU8200). On a top view of SEM images, a number of crossing walls with randomly drawing lines was counted. Averaged wall-to-wall distances were estimated by divisions of the wall counts in the line length. Raman spectra of the CNW samples were acquired using the 532-nm-wavelength laser excitation (Renishaw inVia Raman).

Optical emissions were measured by the spectrometer (Ocean optics, USB2000+) and the optical fiber for evaluation of plasma discharge through the quartz window equipped at the system viewing just beneath of the CCP electrode. The acquisition time was every 1 s.

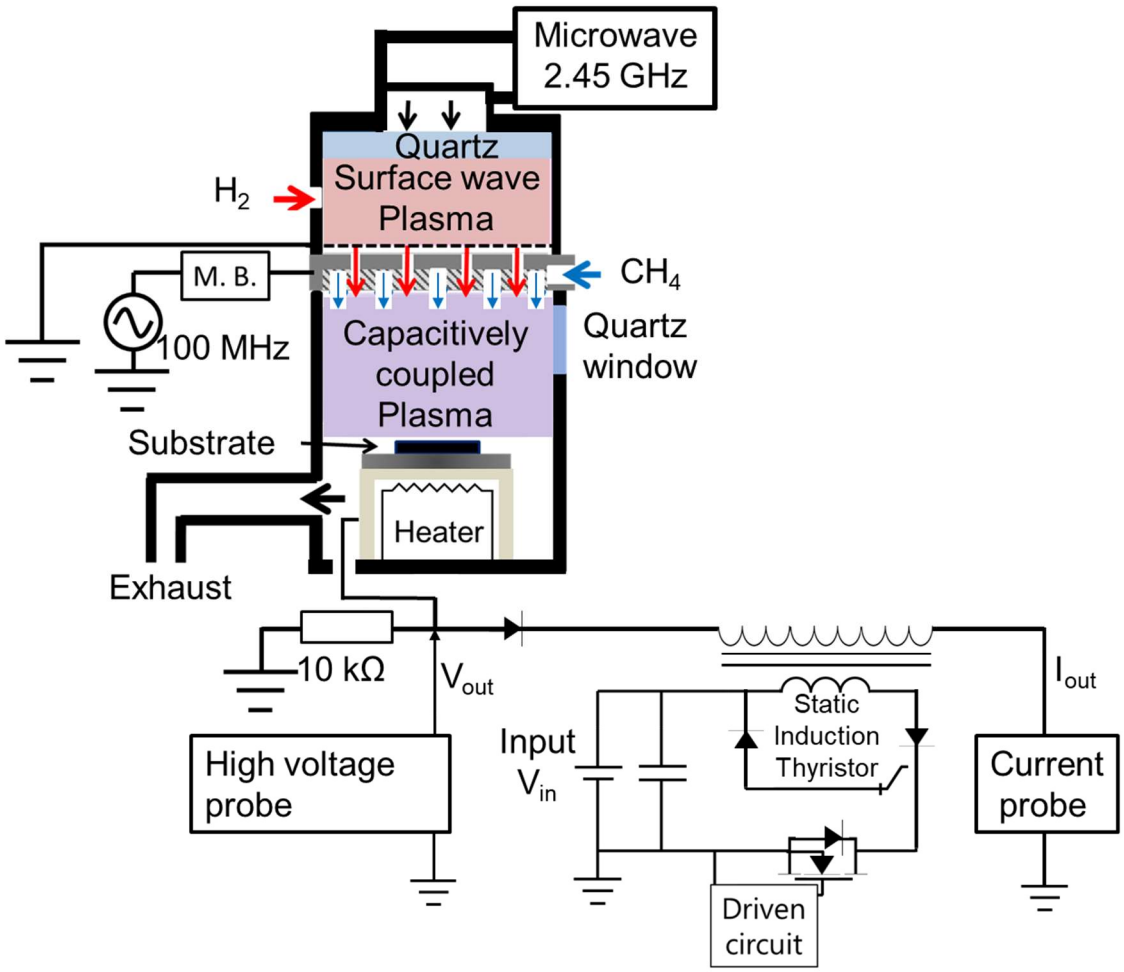

Fig. 5.2.1 Experimental set up of RI-PECVD system with IES circuit. M. B. stands for the impedance matching circuit.

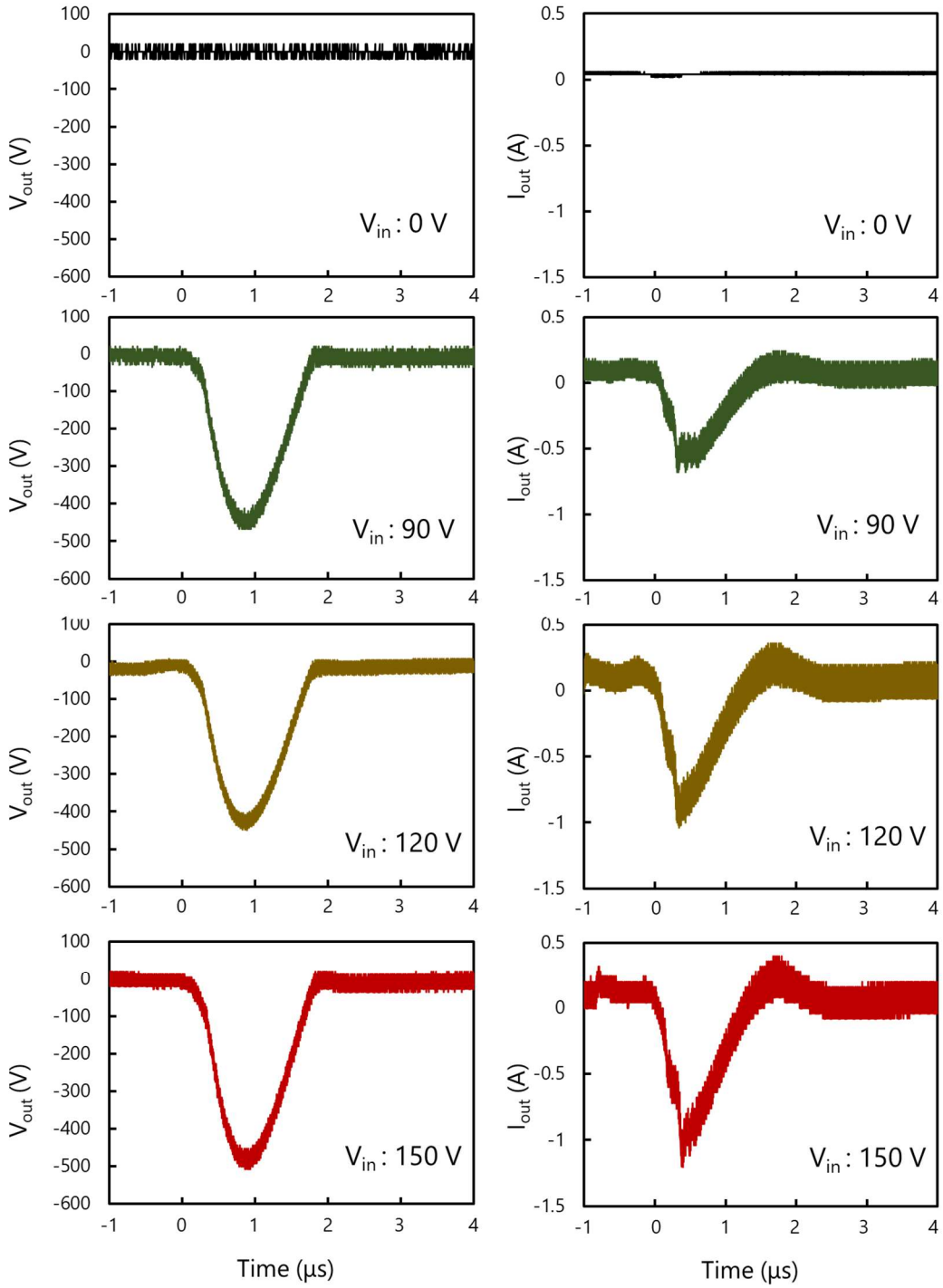

Fig. 5.2.2 The waveforms of one pulse when the high-voltage nanosecond pulse applied at 0, 90, 120, and150 V of the input voltage V_{in}. (a) Output voltage V_{out} and (b) output current I_{out}

Table 5.2.1 Parameters of measured voltages and currents of input and output of the IES circuit.

V （V)	90	120	150
Peak to peak V_{out} (V)	500±40		
Peak to peak I_{out} (A)	0.8±0.2	1.2±0.2	1.4±0.2
Power(W)	58±10	76±10	101±10

5.3 Wall density of CNWs - Effects of high-voltage nanosecond pulses

When the high-voltage nanosecond pulses were applied during deposition, the wall-to-wall distance of CNWs was changed as shown in the SEM images of CNWs [Fig. 5.3.1 (a-d)] and tilted views in [Fig. 5.3.1 (e-h)]. The normally deposited CNWs without the high voltage nanosecond pulses are observed the unique nanostructure of two-dimensional carbon sheets that were grown vertically on the substrate, as shown in Fig. 5.3.1 (a,e). Averaged wall-to-wall distance was approximately 150 nm.

When the high-voltage nanosecond pulses were applied, low-density CNWs films were deposited. As the IES input voltage, V_{in}, increased from 90 to 150 V, the averaged wall-to-wall distances of CNWs extended more sparser than 700 nm. Simultaneously, a number of branches were reduced, as shown in Fig. 5.3.1 (b, c, d). The mean wall-to-wall distances were depended on the V_{in}, as plotted in Fig. 5.3.1 (i). Thus, the dependence of the wall density on the high-voltage nanosecond pulses was apparently seen.

In the tilted views of SEM images as shown at the second row in Fig. 5.3.1, the original surface of substrate was uniformly covered by a layer, in particular of samples prepared with the higher V_{in} application. Fig. 5.3.1 (j) shows the dependence of the total CNWs film thickness and the uniform layer thickness on the V_{in}. The total height of the CNWs films of approximately 500 nm was almost unchanged. When the V_{in} was increased from 90 to 150 V, thicknesses of the uniform-films were increased. For V_{in} of 150V, the thickness reached to approximately 100 nm.

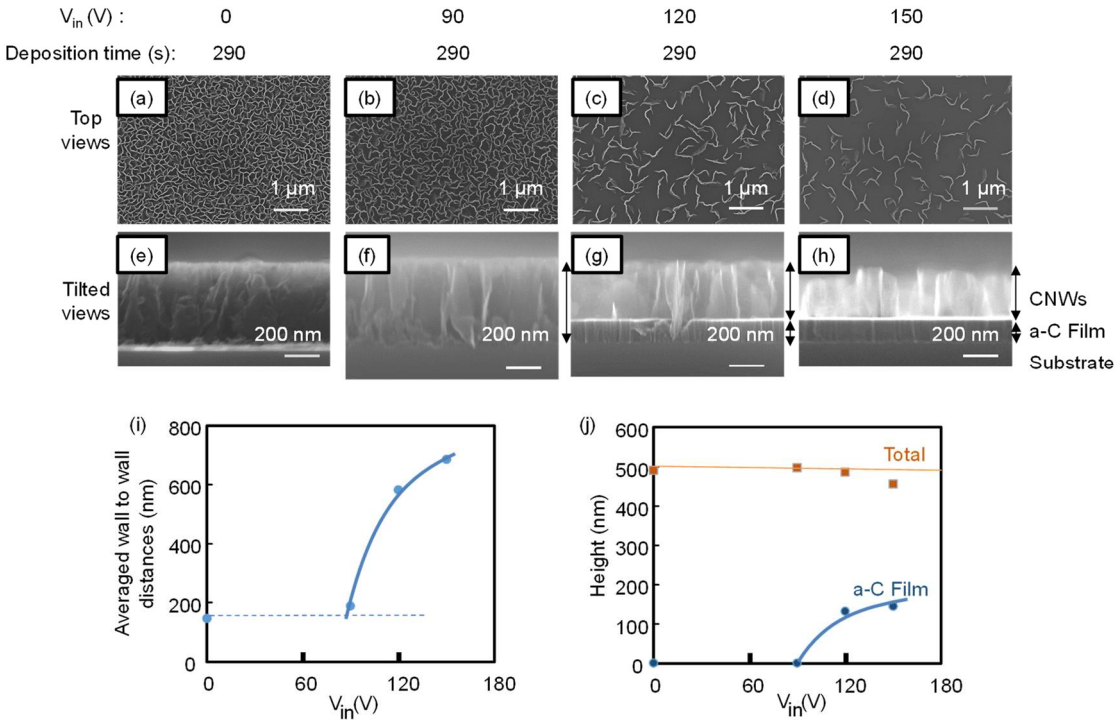

Fig. 5.3.1 SEM images of CNWs. (a - d) The top-views and (e - h) the tilted views of CNWs synthesized using RI-PECVD with high-voltage nanosecond pulse at 0 – 150 V of the input voltage V_{in}. The input current I_{in} is 0.5 A. The input voltage dependence of (i) averaged wall to wall distances and (j) height of the walls of CNWs.

Raman spectra of CNWs are shown in Fig. 5.3.2 (a). As shown in Fig. 5.3.1 (e-h), uniform-films were confirmed. Therefore, Raman spectra was fitted assuming several crystal structures. On the Raman spectra, as shown by dotted lines, a spectral component of the amorphous carbon (a-C) film was overlapped on that of the CNWs film. The component for the CNWs is appeared with peaks at 1590 cm^{-1} (G-band) indicating the formation of a graphitized structure and at 1350 cm^{-1} corresponding to the disorder-induced phonon mode (D-band). Shoulders of the G band are at 1650 cm^{-1} (D'-band). These peaks are commonly observed for the CNW samples.[51] The other peaks are appeared at 2465 cm^{-1}, 2690 cm^{-1} for 2D band, 2945 cm^{-1} for G+D band, and 3240 cm^{-1} for 2G band. The a-C films have two broad peaks at 1350 and 1580 cm^{-1}.[65)–67)] As the V_{in} was increased, the CNW peak components were reduced by thinning out their density. Since the spectral features of the CNWs were similar, crystallinity of the low-density CNWs film was remained and the unique structure of CNWs films was kept even they were synthesized with the high-voltage nanosecond pulses application at higher V_{in} than 120 V. Therefore, this method provides sparsely isolated CNW films with wider average wall-to-wall distance than 700 nm.

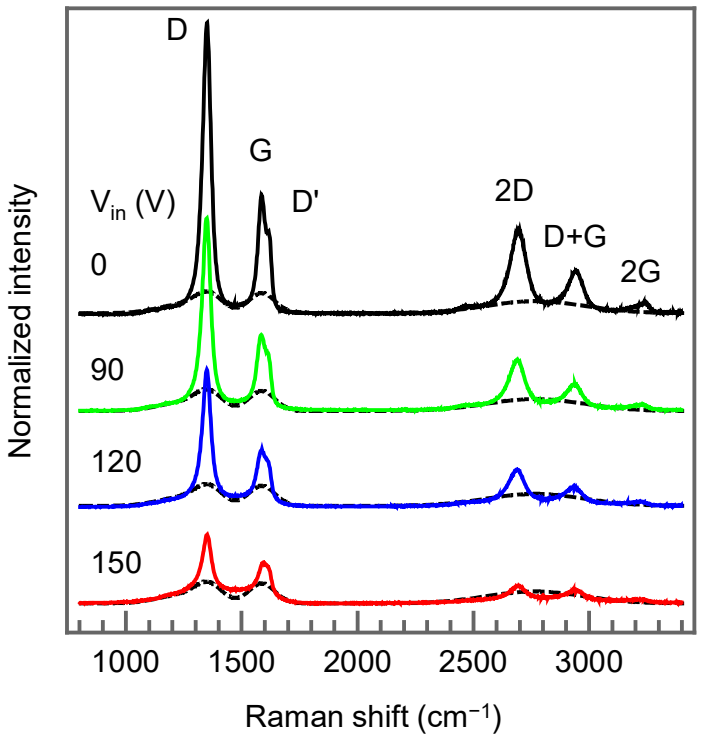

Fig. 5.3.2 (a) Raman spectra and the input voltage dependence of CNWs synthesized using RI-PECVD with high-voltage nanosecond pulse at 0 – 150 V of the input voltage V_{in}.

5.4 Discussion

5.4.1 Plasma parameters

First, effects on plasma discharges were evaluated. Fig. 5.4.1(a) shows normalized optical emission spectra measured at different V_{in}. Intense emissions at a wavelength of 656 and 488 nm were arisen from H Balmer α and β lines, respectively. [68] In addition, the emission line at 431 nm was originated from CH ($A^2\Delta$-$X^2\Pi$) transition. The C_2 Swan band ($A^3\Pi_g$—$X^3\Pi_u$) emissions are not apparently observed around 563, 516, 473, and 437 nm. In the ranges from 450 to 640 nm and from 720 to 750 nm, emissions of molecule H_2 were clearly observed.[69]

Dissociation degrees of CH_4 and electron temperature of the CH_4/H_2 plasma were roughly evaluated by taking ratios of emission intensities. Fig. 5.4.1 (b) shows the V_{in}-dependence of time-averaged emission intensity ratios of CH/H_α and H_β/H_α. The ratios were not changed drastically by changing V_{in}. This indicates that bulk plasma parameters were not significantly changed by the high-voltage nanosecond pulse application.

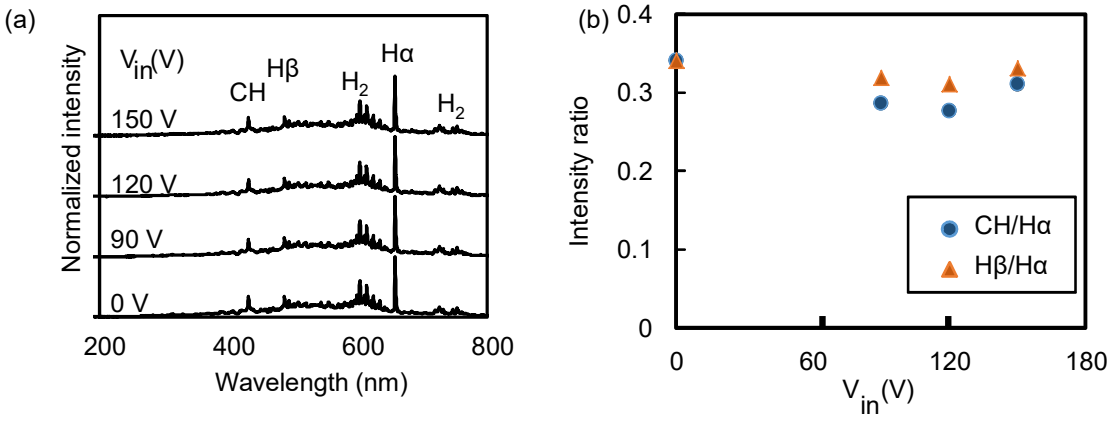

Fig. 5.4.1 The input voltage dependence of (a) OES spectra. Intensity ratios of (b) CH and (c) H_β referred to H_α.

5.4.2 Temporal dependence in deposition

In the conventional growth without the high-voltage nanosecond pulse application, densely interconnected CNWs are observed even after the deposition for 60s. At the early stage 60 s of the CNW growth, the effect of high-voltage nanosecond pulse (V_{in} = 150 V and I_{in} = 0.5 A) was investigated. Even at the early stage of deposition for 60 s, the sparsely isolated CNWs are observed with high-voltage nanosecond pulse application, as shown in Fig. 5.4.2 (a,c,e). As further CNW growth at 180 s, the CNWs density reduced significantly and the uniformly covered a-C film thickness was almost linearly increased, as shown in Fig. 5.4.2 (b,d). The CNWs were buried in the a-C films.

The time dependence of thicknesses of total CNWs film and the a-C film is plotted in Fig. 5.4.2 (f). Considered with the linear dependences of the film thickness on the deposition time, the fluxes of carbon precursors were sustained regardless of application of the high voltage nanosecond pulses. However, since the ion flux is modulated, the CNW growth is possibly inhibited as follows: First, the high-voltage nanosecond pulses sweep away electrons from plasma and then the ion matrix is formed. In the ion matrix, ion flux for bombardment to the surface is increased. This enhances to form a number of active sites on the surface, leading to adsorb gaseous carbon radicals without surface diffusions. Normally, the carbon diffused on the surface until trapping at the active sites. To reduce the surface diffusion lengths and is to reduce the radicals for making nucleus and inhibit nucleation of the CNW. Oppositely, a-C films are enhanced to grow as similar as higher ion flux conditions. As shown in Fig. 5.4.3, the a-C film in thickness was thinner, when V_{in} was lower voltages.

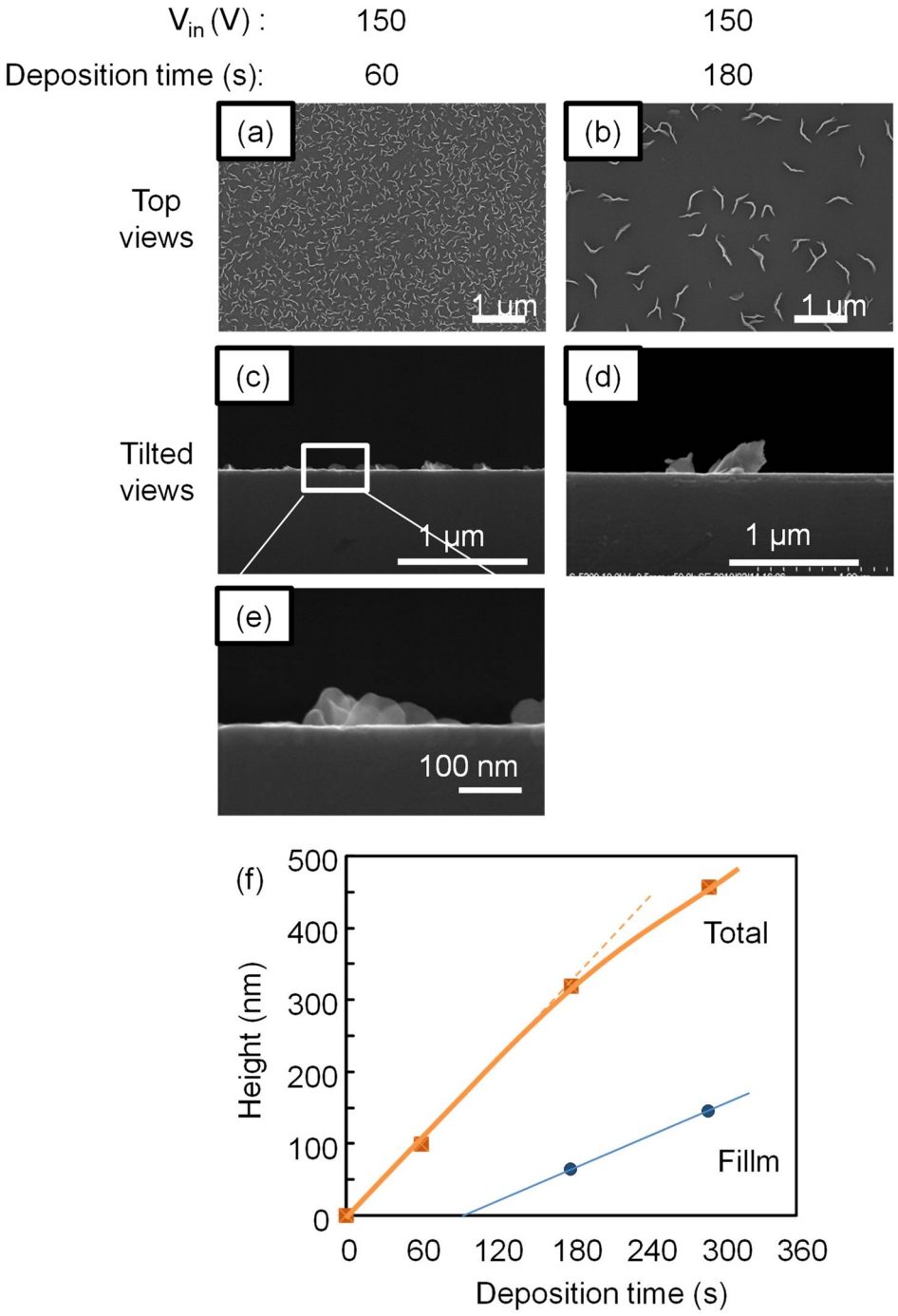

Fig. 5.4.2 The depositions time dependence of SEM images of CNWs synthesized with high-voltage nanosecond pulse at 150 V of the input voltage and 0.5 A of the input current. The top views for deposition time at (a) 60, and (b) 180 s. Tilted views for (c) 60, and (d) 180 s and enlarged view (e). (f) The deposition time dependence of thicknesses of total CNWs film and a-C film.

5.4.3 Effect of pre-deposited CNWs

Regrowth of dense or sparse CNWs was evaluated. Initially, low height CNWs films were deposited by the condition with high-voltage nanosecond pulse application using 150 V of V_{in}. The sparsely isolated CNWs films were grown by subsequent growth of the normal condition without the high-voltage nanosecond pulse application by the growth of CNWs film for 60 and 180 s. The longer deposition time resulted lower CNWs density. Fig. 5.4.3 shows the SEM image of CNWs synthesized after growth with high-voltage nanosecond pulse at 150 V of the input voltage V_{in}. The subsequent growth of CNWs produced dense CNWs film. Although the a-C film was uniformly covered on whole surface of the substrate, the normal condition grew only the CNWs film. It is noticeable that heights of CNWs were uniformly grown at a uniform as shown in Fig. 5.4.3 (a,d). This indicates that CNWs are grown under the normal condition without the high-voltage nanosecond pulse application. As the consequence, the densely grown CNW was thinned out to from isolated sparsely wall-like structures.

Interestingly, the subsequent growth of CNWs without the high-voltage nanosecond pulse application was on the pre-deposited sparse CNWs substrate prepared using nanosecond pule application with 150 V of V_{in} at 180 s were grown at different height as shown in Fig. 5.4.3 (b,c,e). The pre-deposited CNWs grew linearly depending on the deposition time.

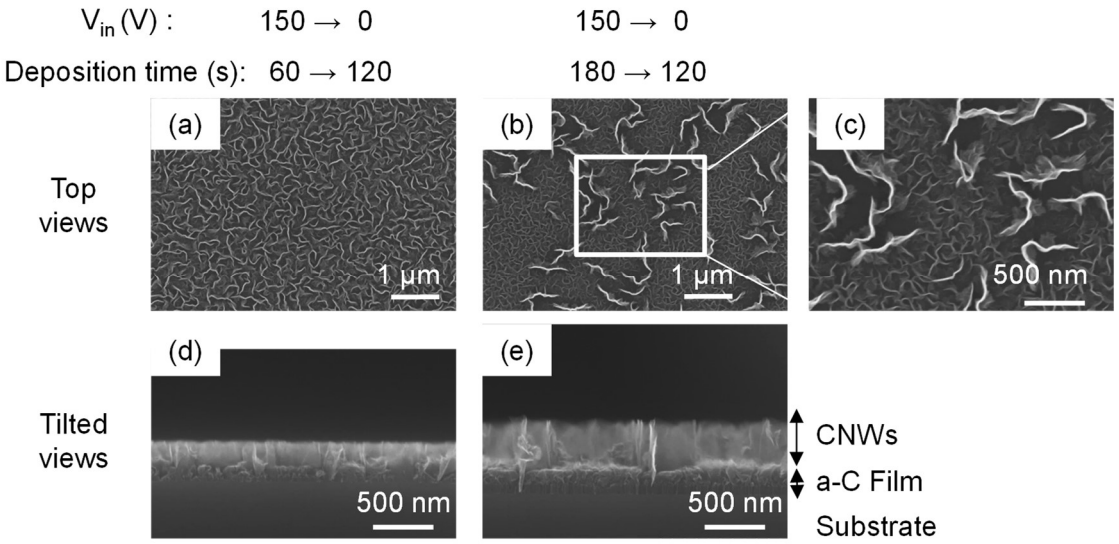

Fig. 5.4.3 SEM images of CNWs synthesized using RI-PECVD without bias at 120 s after growth with high-voltage nanosecond pulse at 150 V of the input voltage V_{in} at 60 s [(a) top view and (d) tilted view] and 180 s [(b) top view and (c), (e) tilted view].

5.4.4 Comparison with the previous literatures

A number of reports about growth or synthesis of CNW or vertical oriented graphene nanosheets has been published previously. The averaged wall-to-wall distances and deposition parameters are tabulated in Table 5.4.1. Cho et al. reported about the effect of gas pressure and plasma excitation power injected into plasma on the synthesis of CNWs using the RI-PECVD system with CH_4 and H_2 gases.[11] The averaged wall-to-wall distance were the narrowest of 50 nm at deposition pressure of 1 Pa, while at the widest of 200 nm at a pressure of 3 Pa. Additionally, the averaged wall-to-wall distance became to widen 300 nm by application of high excitation power of 400 W. Suzuki et al. reported that the wall-to-wall distance of CNWs was changed from 20 to 150 nm by application of substrate bias with radio frequency or direct current power in radical injection PECVD (RI-PECVD) with C_2F_6 and H_2 gases.[70] The Dinescu group reported that the densely CNW film with average wall-to-wall distance of approximately 200 nm was synthesized at stage temperature of 700 °C in downstream of plasma in a mixture of $Ar/H_2/C_2H_2$ gases at pressure of 110 Pa.[71),72] In that experiment, they observed spontaneous transition of growth regimes from carbon nanotube to CNW. Gupta et al. analyzed the CNW sheet growth on CNT substrate on the basis of surface adsorption of plasma-generated species.[73]

Morphological characters in relation with the CNW are categorized into each zone on the growth conditions representing like a contour plot, as proposed by Kondo et al. The growth zones are proposed to be segmented by two parameters of mean ion energy and total ion flux.[72] As the mean ion energy is lower than the threshold around 150 eV, no nucleation of carbon sheets occurs. Oppositely, as exceeded the energy around 250 eV, etching of the graphene sheets occurs. Besides, an optimum range for CNW growth is segmented by boundaries between no deposition (below 2.5 μA cm^{-2} ~ 1.6×10^{13} cm^{-2} s^{-1}) and a continuous film growth (above 4.5 μA cm^{-2} ~ 2.8×10^{13} cm^{-2} s^{-1}).[13] The interconnected wall-like structure with the averaged wall-to-wall distances ranged from 20 to 200 nm was segmented from the a-C film formation or no film deposition. In this study, it was realized to grow the sparsely isolated CNW with wide distances on conventional precursors and silicon substrate.

Table 5.4.1 A list of the averaged wall-to-wall distance of CNW films in the selected publications. PECVD: plasma enhanced chemical vapor deposition; RI: Radical injection; HV: high voltage; ns: nanosecond; RF: Radio frequency; DC: Direct current; MW: Microwave; ICP: Inductively coupled plasma; EBEP: Electron beam excited plasma; PA: Plasma assisted; DCB: 1,2-dichlorobenzene

Method	Sources	Pressure (Pa)	Stage temperature (C)	Averaged wall-to-wall distance (nm)	Refs.
RIPECVD + HV ns pulse	CH_4. H_2	1	650	700	This study
RIPECVD	CH_4. H_2	1	600	300	Cho (2014)
RIPECVD	C_2F_6, H_2	160	580	30	Kondo (2005); Takeuchi (2009)
RF PECVD	C_2F_6, H_2	13	500	100-300	Hiramatsu (2004); Hiramatsu (2006)
RF PECVD	CH_4. H_2	13	680	300	Zhu (2007)
RF PECVD	CH_4. H_2	12	600-900	~500	Wang (2004)
DC PECVD	CH_4. H_2, Ar	2.8	550-750	200	Kobayashi (2007)
MW PECVD	CH_4. H_2	133	650-700	~500	Wu (2002)
MW PECVD	CH_4, N_2, Ar	1333	1150	~500	Cheng (2012)
ICP CVD	C_2H_2, Ar	1	255- 400	-300	Jain (2011)
EBEP	CH_4. H_2	4	570	-200	Mori (2008)
Remote PECVD	C_2H_2, H_2, Ar	100	700	200-500	Vizireanu (2008); Mozetic (2015); Vizireanu (2017)
Furnace PA CVD	CH_4. H_2, Ar	>7	520-550	-300	Li (2019)
Furnace PACVD	DCB, CH_4		60-100	>500	Hsu (2017)

5.4.5 A model of growth of CNWs films

The results of this study are summarized as follows:

(1) The high-voltage nanosecond pulse application inhibits to grow densely the CNWs,

(2) The powers of the high-voltage nanosecond pulses determined the effect of inhibition of the CNW growth, depending on amounts of the swept electrons,

(3) In the short-period after the high-voltage nanosecond pulses, ion bombardments enhance to adsorb radicals as deposited precursors, leading to cover uniformly a-C films on the surface of substrate,

(4) Tips or edges of the pre-deposited CNWs grow in the period during no application of the high-voltage nanosecond pulse, namely, efficiency of deposition onto the pre-depositing CNWs is usually higher than that of the flat areas,

(5) Crystallinity of the CNWs is not regard with the high-voltage nanosecond pulse application.

From the above-stated summary of these experimental results, the author reconsiders the main processes of CNW growth, as illustrated in Fig. 5.4.4. In the low-pressure weakly ionized plasma discharges, carbon precursors are generated electro-impact induced reaction. For instance, carbon atom adsorbs and deposits of influx from plasma to surface. During surface diffusion of the adsorbed atom, it is incorporated at active sites. First, nucleation for wall growth occurs and then the CNW at the tips or the edges act as the active sites. This is asserted by the incorporation at the tips or the edges of the pre-deposited CNW is highly efficient processed as compared with deposition of carbon atom at the flat areas.

The growth model as proposed by Kondo et al. clarifies this sequence, presenting in the observed results of the initial growth process of CNW.[19] At the first stage, adsorptions of these $\cdot CH_3$ or $\cdot CF_3$ and H radicals on a surface occur with a form of Langmuir isotherm. The sequential growth mechanism is comprised: (1) uniformly covered carbon buffer layer formation, (2) defect formation on the buffer layer for clustering of nano-islands, (3) sparsely dispersed nanographene sheets growth at edges of the islands, and (4) vertical growth of nanographene sheets.[61] Moreover, the nucleation or clustering process plays a key role for vertical growth of CNW. Lehmann et al. were observed enhancement of vertical growth originating at cracks at grain boundaries, when polycrystalline titanium nitride (TiN) substrate was used.[74] Ghosh et al. discussed the

defect generation on the surface of graphene sheets.[75)–79)] For the other explanations, Cheng and Teii suggested that horizontally aligned growth until horizontally grown graphene sheets touched each other, later raise and grow vertically due to the lack of space.[80),81)] After all, Zhu et al. pointed out that the key processes are energetically favored to adsorb edge rather than side of the graphene sheets, because the adsorbed radicals can diffuse along the edge and side of the sheets for long time.[82)]

In the surface diffusion process, Levchenko et al. assumed that carbon atom adsorbed on the carbon layer and the adsorbed carbon atom diffused along two directions, namely, side and edge of vertical graphene sheets.[61)] Surface diffusion length of carbon atom on pure graphite surface, where it can migrate along a surface before being re-evaporated, was estimated by $\lambda_d = 2\ a_0 \exp[(E_a - E_d)/2kT_s] = 3.7\ \mu m$, where atomic radii, $a_0 = 0.1$ nm, surface temperature, $T_s = 1000$ K, and the Boltzmann constant $k = 1.381\times10^{-23}$ J/K or 8.62×10^{-5} eV/K.[82)] Thus, adsorbed carbon precursors can ideally migrate enough long distances on the surface.

The radical surface diffusion is immediately terminated by ion bombardments. The radical attachment may be gained to the place at flat instead of the nanosheet edges. In fact, the growth rate is governed by ion flux toward the surface, as similarly in the case of the nanomaterial growth.[83)] Giese et al. focused on surface temperature and ion-energies. They summarized the growth zones of CNW growth based on consideration of surface diffusion moving adjacent adsorption sites on the surface.[84)] At the steady-state condition of the sheet growth, influx of carbon atom is balanced with the ion-induced carbon atom adsorption onto edges of the sheets. Simply, fluxes of both radical and ion are determined the sheet growth in a stationary phase.[61)] Thus, the nucleation and edge-termination processes are taken into account that the high-voltage nanosecond pulses are repeatedly disturbed these flux balance.

The plasma-generated radicals are continuously exposed for adsorption. In contrast, under circumstances of highly energetic ions bombardments on the surface, sputtering process can remove or evaporate the adsorbed atom. The ion bombardments are regulated the surface processes of diffusion, nucleation, and sheet-growth, simultaneously. However, the surface processes have not been separately activated by the continuous application of the biasing.

Here in practice, the steady-state plasma was modulated by the nanosecond pulse

at a time-scale of 100 nanosecond. During the 100-nanosecond pulse application, the high-voltage swept away a large fraction of electrons from the discharge regions, as reported Pustylnink et al..[62] The ion-matrix was formed and the ion bombardments toward the surface modulated the radical adsorption affecting to the CNWs growth. In this study, the repeated modulations in a short period of nanosecond pulses could be separately controlled these surface processes, in regard with the ion bombardments. It was ensured that the high-voltage nanosecond pulse application swept electrons for short period. Therefore, only modification of the growth processes takes place.

Lastly, the high-voltage nanosecond pulse application inhibits the wall growth, owing to enhance adsorption of carbon atom and regulate surface diffusion lengths. As the result, the growth at the tips or edges of CNW is regulated to form the sparse CNW films. Characteristically, the wall-to-wall distances of CNWs films were changed under the high-voltage nanosecond pulse applications. Furthermore, this study established the novel processing for deposition by the low-pressure plasma with high-voltage nanosecond pulse. The method of controlling wall density of CNWs films is expected to utilize for realizing nanographene applications.

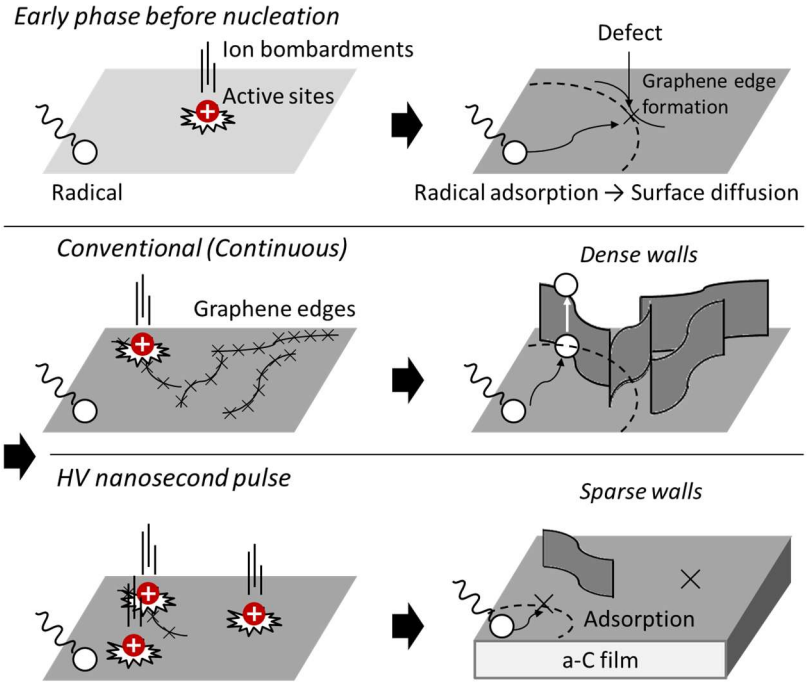

Fig. 5.4.4 Temporal changes in the CNWs film growth for one cycle of the high-voltage nanosecond pulse application. The high-voltage pulse swept away electrons and then the ion bombardments enhanced to adsorb radicals by generation of a number of active sites. Also, tips or edges were grown significantly faster than that of flat areas, leading to form wall-like or flake structures.

5.5 Conclusions of this chapter

CNWs were synthesized using a RI-PECVD system equipped with the inductive energy storage (IES) circuit. When the IES circuit connected to the stage electrode and applied high-voltage nanosecond pulses, this study found that the CNW films were sparsely grown with widely averaged wall-to-wall distances by changing the stored electrostatic powers. Almost as if the high-voltage nanosecond pulses were mowing the nucleation of seeds for CNW growth. In terms that the high-voltage nanosecond pulses can be swept away electrons from the plasma in a short period as it was applied, ion bombardments toward the surface of substrate might be modulated leading to adsorb the carbon precursors that were generated in gaseous plasma. In continuous plasma deposition, the steady state CNW growth is considered to three stages of (i) surface diffusion along the side, (ii) nucleation of graphene sheets, then (iii) deposition of carbon precursors at edges of graphene sheets. The ion-bombarded modulation induced to adsorb the diffused carbon precursors at ion-activated sites. As a result, the adsorption efficiency increased to inhibit the surface diffusions enough for long time, causing to deposit the a-C film covered uniformly on the ground surface, and leading to grow the CNW films with mowing sparsely the carbon walls, i.e., it was wider averaged wall-to-wall distances of the CNW films.

Chapter 6 Scaffolds with isolated carbon nanowalls promote osteogenic differentiation through Runt-related transcription factor 2 and osteocalcin gene expression of osteoblast-like cells

6.1 Introduction

It is reported that the differentiation of Saos-2 cells was significantly up-regulated when the cells were incubated on CNW scaffolds with average wall-to-wall distances ranging from 200 to 400 nm in Chapter 3.

Typically, it is only possible to control narrow wall-to-wall distances using the RI-PECVD system.[11] However, isolated CNWs were fabricated with average wall-to-wall distances of over 1 μm by the application of nanosecond pulse voltages onto the growth substrate as shown in Chapter 5. This technology allows the control of wall-to-wall distances, with CNWs prepared with wall-to-wall distances ranging from 100 to 3300 nm that were subsequently employed as scaffolds for cell culture.

This study demonstrated the utility of sparse isolated CNWs with average wall-to-wall distances from 100 to 3300 nm as scaffolds for culturing osteosarcoma Saos-2 cells. Cell morphology was observed, and proliferation and differentiation were evaluated by the gene expression of proliferating and differentiating osteogenic cells using the real-time PCR. All scaffolds were prepared using CNWs synthesized by a RI-PECVD system. Controlling the repetition rates of the nanosecond pulses and maintaining a constant electrostatic input provided CNWs with average wall-to-wall distances ranging from 100 to 3300 nm. The substrate holder (32 cm^2) was electrically connected to the inductive energy storage (IES) circuit. Details of the RI-PECVD system with the IES circuit are shown in chapter 5. The synthesis conditions for the CNW scaffolds used for cell culture are shown in Table 6.1.1. Differences in cell morphology and cell viability using CNWs with various wall-to-wall distances were studied.

Table 6.1.1 Conditions and features of CNWs synthesized using RI-PECVD with high-voltage nanosecond pulse at Condition I (D = 3300 nm), Condition II (D = 700 nm), and Condition III (D = 100 nm)

Condition Wall-to-wall distance, *D* (nm)	I 3300	II 700	III 100
Pressure (Pa)	1		
H_2 (sccm)	100		
CH_4 (sccm)	50		
Microwave power applied to SWP (W)	400		
VHF power applied to CCP (W)	400		
Distance between CCP electrodes (mm)	30		
Temperature of substrate (℃)	650		
Deposition time	4 min 50 sec		
Substrate	Si (100)		
Input of DC voltage to IES circuit (V)	150	150	0
Input current to IES circuit (A)	0.5	0.5	0
Pulse repetition rate (kpps)	20	50	-
Total height (nm)	465	456	491
a-C film (nm)	101	145	0
I_D/I_G	1.9	2.4	3.0
Measured wall-to-wall distances (nm)	3286	685	146

6.2 Experimental details

Saos-2 cells were incubated in Dulbecco's modified Eagle's medium (DMEM) (Sigma, D5796) in a humidified atmosphere of 5% CO_2/95% air at 37 °C. The experimental setup for culturing cells on CNW scaffolds was previously described.10 A 48-well cell culture cluster (Corning, 3548) made from polystyrene (PS) was used for incubation as a control. Before cell culture, all components were washed with pure water and sterilized by exposure to ultraviolet light for 20 min. The wells were filled with 300 μl phosphate-buffered saline (PBS; Gibco Life Technologies) for 20 min, and then the PBS was replaced with fresh PBS for 15 min. Thereafter, each well was filled with 300 μl DMEM supplemented with 10% fetal bovine serum (Life Technologies, 10437-028), 100 units/ml penicillin, and 100 μg/ml streptomycin (Life Technologies, 15140-122) and left for 1 h at room temperature. A total of 3000 cells were seeded in each well.

Cell viability was evaluated after 4 days' incubation. The measurement of cell viability was described in 2.3.

Mitochondria within the cells were observed by the method shown in 2.5.2, after 4 days' incubation.

Real-time PCR, as described in Chapter 2.4, was used to detect mRNAs encoding Runt-related transcription factor 2 (Runx2) and osteocalcin (OC) after 10 days' incubation. Cells were seeded at around 1×10^5/well.

The morphological features of the cells were observed after incubation for 1 and 2 days. The cells were fixed by the method as shown in Fig. 2.5.1. Actin cytoskeleton was stained with 100 nM Acti-stain^{TM} 488 phalloidin and nuclei were stained with 200 nM DAPI as shown in Figs. 2.5.3 and 2.5.4.

CNW scaffolds were prepared with average wall-to-wall distances (D) ranging from 100 to 3300 nm. Fig. 6.2.1 shows top and tilted views of SEM images of the synthesized CNWs: (a) and (d) condition I (D = 3300 nm), (b) and (e) condition II (D = 700 nm), and (c) and (f) condition III (D = 100 nm). The heights of the CNWs were ~500 nm. The a-C film uniformly covered the substrate in conditions I and II, as reported in Chapter 5. The water contact angles on all CNWs were about 40–70 deg. Dowling et al. reported that highly hydrophilic or hydrophobic surfaces led to a progressive reduction in the level of adhesion of osteoblast-like cells.[85] Hence, all CNWs were expected to adhere cells.

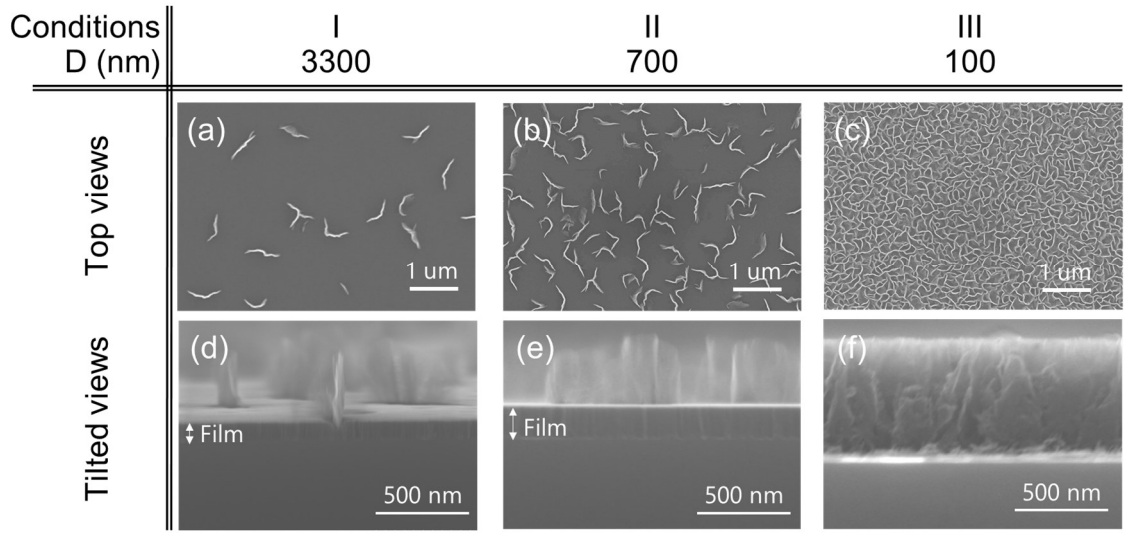

Fig. 6.2.1 Characteristics of the CNWs. SEM images of CNWs. (a - c) Top-views and (d - f) tilted views of CNWs synthesized using RI-PECVD with high-voltage nanosecond pulses at (a, d) Condition I (D = 3300 nm), (b, e) Condition II (D = 700 nm) and (c, f) Condition III (D = 100 nm).

6.3 Results

Saos-2 cells were cultured on the CNW scaffolds. Fig. 6.3.1 shows fluorescence microscope images of cell nuclei and F actin in Saos-2 cells grown on PS and the CNW scaffolds with different D's (D = 3300, 700, and 100 nm) after incubation for 2 days. The cells adhered on all the CNW scaffolds. The fluorescent areas on the microscopic images were counted using the image processing program ImageJ.

Fig. 6.3.2 (a) shows the cell-fluorescent areas of the PS support and the CNW scaffolds with different D's (D = 3300, 700, and 100 nm) after incubation for 2 days. The cell-fluorescent areas indicated the extensibility of the cells. The CNW scaffolds with D = 100 nm had the smallest area of cell growth of the conditions tested. Cell growth on the sparse CNW scaffolds with D = 3300 nm was similar to that on flat PS. The CNW surfaces showed good biocompatibility because cell extensibility and adhesion were unchanged, suggesting that the CNW edges determine cell extension and cell culture was successful.

Fig. 6.3.2 (b) shows the number of cells incubated on the CNW scaffolds (D = 3300, 700, and 100 nm) after 4 days' incubation. Although the largest number of cells grew on the PS surface (a commercial dish for culturing cells), the number of cells on all the CNW scaffolds was not significantly different, at 1×10^5 to 2×10^5 cells. Thus, sparse, isolated CNW scaffolds do not affect cell proliferation compared to dense CNW scaffolds. Cells on all the CNWs scaffolds adhered similarly regardless of the wall-to-wall distances.

The expression levels of Runx2 and OC were used as indicators of cell differentiation. Fig. 6.3.3 (a) shows the relative expression levels of Runx2/RPS18 after incubating the cells under the indicated various conditions for 10 days. The relative expression levels were highest for the D = 700 nm CNW scaffolds. The normalized levels were 1.0 for PS and 3.4 for D = 3300 nm, 8.1 for D = 700 nm, and 2.2 for D = 100 nm for the CNW scaffolds. These differences were significant for all the CNW conditions ($p < 0.05$). Similarly, Fig. 6.3.3 (b) shows the relative expression levels of OC/RPS18 after incubation for 10 days. The normalized expression levels were 1.0 for PS and 4.1 for D = 3300 nm, 8.4 for D = 700 nm, and 2.3 for D = 100 nm. These differences were significant for all the CNW conditions ($p < 0.05$). Interestingly, differentiation of Saos-2 cells was promoted by the middle wall-to-wall distance CNW scaffolds (D = 700 nm).

These results indicate that the effect of the CNW scaffolds on cell differentiation increases with increasing D, consistent with previous research on culturing cells on

CNWs with D ranging from 200 to 400 nm as shown in Chapter 4. However, differentiation decreases as D approaches the size of cells, such as D = 3300 nm. Thus, CNWs with optimal D promote the differentiation of cells.

Fig. 6.3.4 shows top and tilted SEM images of cells grown on Si and CNW scaffolds with different D's (D = 3300, 700, and 100 nm). The white arrows indicate the cell regions shown in the top views [rows (a) and (b) of Fig. 6.3.4], in color. Rounded cells were observed for the dense CNW scaffolds with D = 100 nm. In the enlarged views [row (b) of Fig. 6.3.4], the morphology of the cells shows polygonal shapes and filopodia on the edge of the CNW scaffolds with D = 700 and 100 nm. Smooth curved cell boundaries are seen for the flat Si and the sparsely CNW scaffolds with D= 3300 nm. The filopodia act as tentacles to sense the environment. CNWs with D = 700 and 100 nm appear to influence the morphology of the cells, and the cells formed filopodia to sense the walls. Fig. 6.3.4 (c) and (d) show tilted views of SEM images of the cells. The cells adhered to the scaffold, especially on the flat Si scaffold surface and the spare CNW scaffold with D = 3300 nm. With dense CNW scaffolds, the wall-to-wall separation was too narrow to allow the cells to adhere to each wall, and thus, adhesion of the cells appeared to be suppressed. Notably, the walls acted like a wedge, and the cells adhered on the CNW scaffold with D = 700 nm, as indicated with red arrows in row (d) of Fig. 6.3.4. Thus, the CNW scaffold with D = 3300 nm was not effective for cell adhesion, and the scaffold with D = 100 nm was too narrow to affect the scaffold morphology. The CNW scaffold with D = 700 nm had a large effect on cell adhesion, promoting osteogenic differentiation.

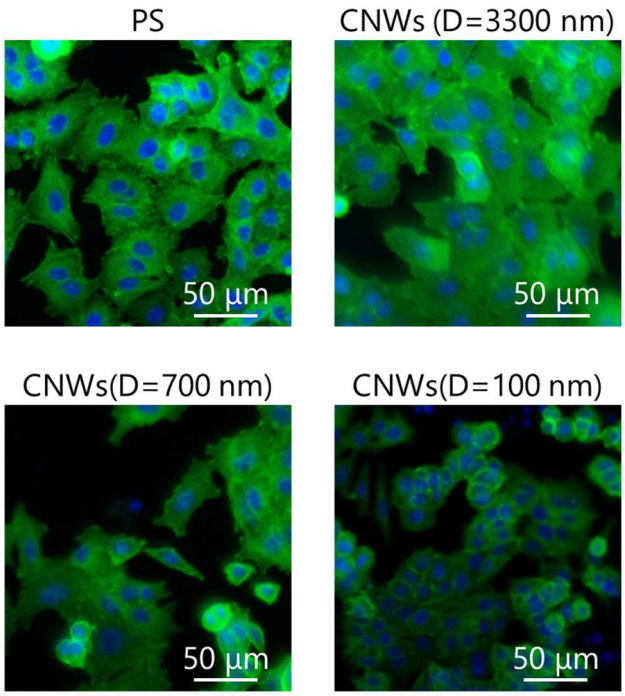

Fig. 6.3.1 Fluorescence microscope images of cells stained with DAPI and Acti-stain 488 phalloidin solution grown on (i) PS and CNW scaffolds with different D's (D = 3300 nm, 700 nm and 100 nm) after incubation for 2 days. (Contd.)

(a)

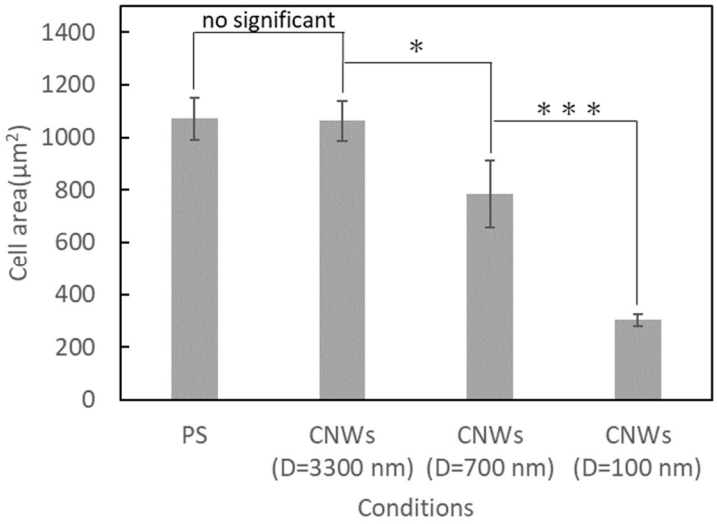

(b)

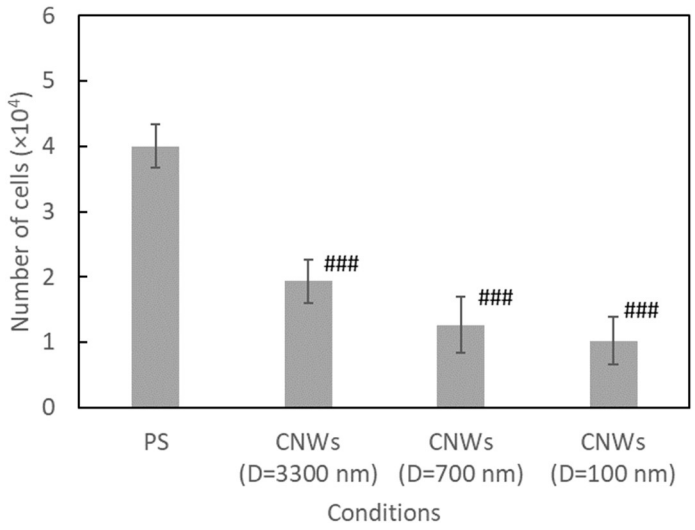

Fig. 6.3.2 (a) The area per cell calculated from the fluorescence microscope images. (n = 15, *: $p<0.05$, ***: $p<0.005$). (b) Number of cells determined using the MTS assay on PS and the CNW scaffolds with different D's (D = 3300 nm, 700 nm and 100 nm) after incubation for 4 days (n = 4, ###: $p<0.005$ compared to the number of cells cultured on PS).

(a)

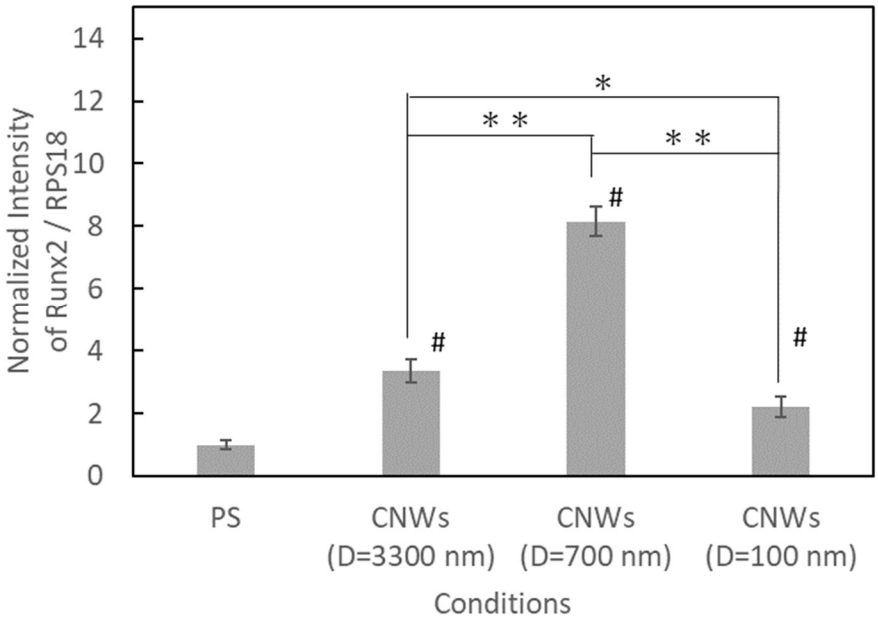

(b)

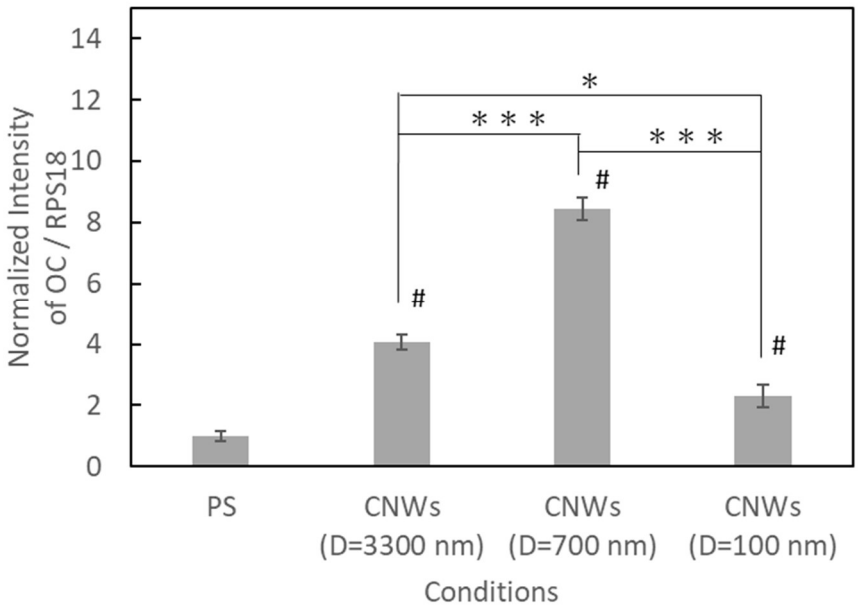

Fig. 6.3.3 Relative levels of bone marker expression determined using real-time PCR after incubation for 10 days. (a) Runx2 and (b) OC following culture on PS and the CNW scaffolds with different D's (D = 3300 nm, 700 nm and 100 nm) (N = 3, *: $p<0.05$, ***: $p<0.005$, #: $p<0.05$ compared to the expression levels of cells cultured on PS).

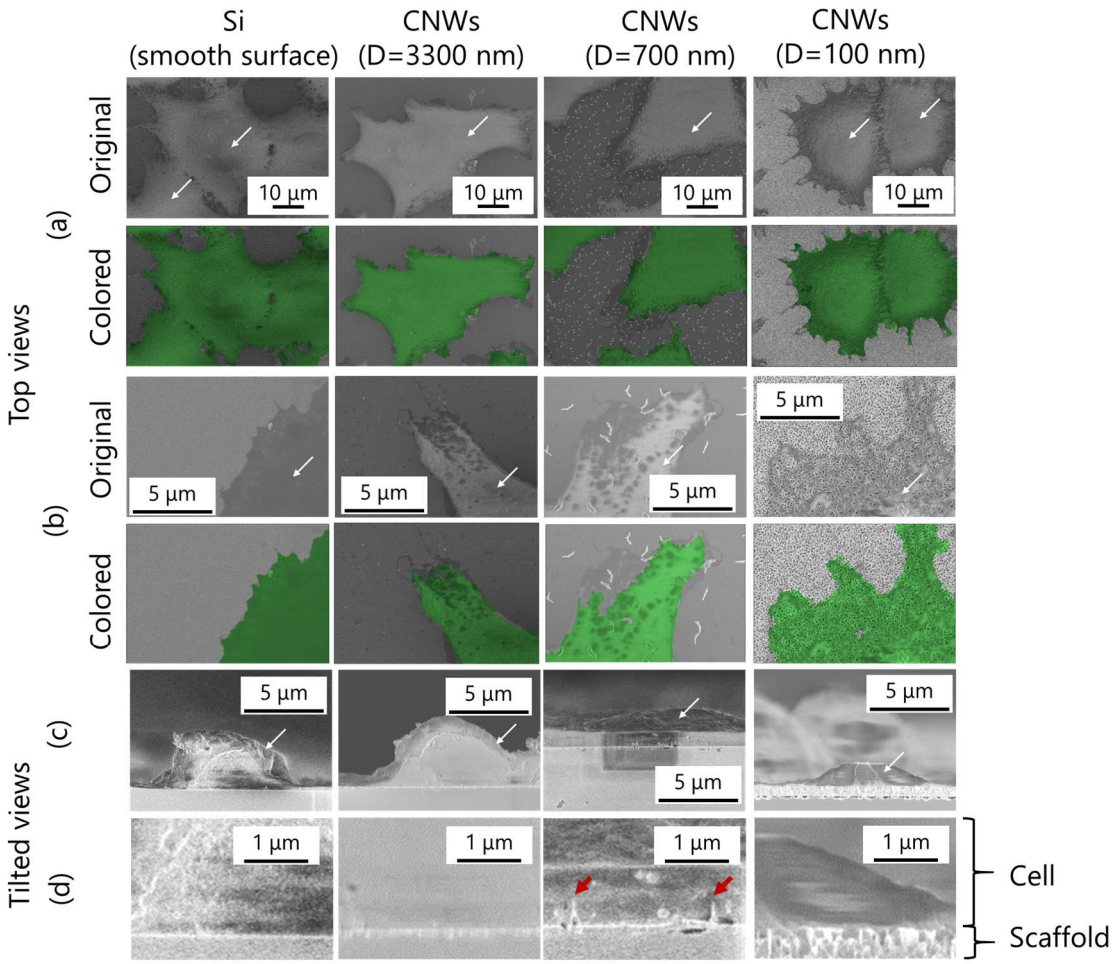

Fig. 6.3.4 (a), (b) The top views and (c), (d) the tilted views of SEM images of cells fixed after 2 days' culture on Si and CNW scaffolds with different D's (D = 3300 nm, 700 nm, and 100 nm). The white arrows indicate parts of cells.

6.4 Discussion

The cytoskeleton affects to osteogenic signaling of cells. In topography-induced osteogenesis, the nano- or micro-topography of scaffolds activates several pathways of osteogenic differentiation, including the mitogen activated protein kinase (MAPK) pathway, focal adhesion kinase (FAK) activation, bone morphogenetic proteins (BMPs), and the Wnt/β-catenin pathway, as reported by Rougerie et al..[86] Growing cells on a scaffold composed of poly(ethylenimine)-conjected graphene oxide (PCL_GO) reduced the cell area and promoted osteogenic differentiation of hMSC cells, as reported by Kumar et al.[87] , and the distribution of focal adhesion (FA) was expressed at the tips of cellular protrusions of cells cultured on PCL_GO. Nano-roughed surfaces also reduced the cell area, changed the distribution of FA, and promoted the osteogenic differentiation of cells, as reported by Hasan et al..[88] In the present study, cell morphogenesis on the CNW scaffold with D = 700 nm led to osteogenic differentiation. This result suggests that the distribution of FA in cells cultured on the CNW scaffold with D = 700 nm uniquely promotes the differentiation of cells. Fig. 6.4.1 illustrates the results of this experiment. The morphology of adhesive cells cultured on the CNW scaffold with D = 700 nm favors activation of the pathway of osteogenic differentiation.

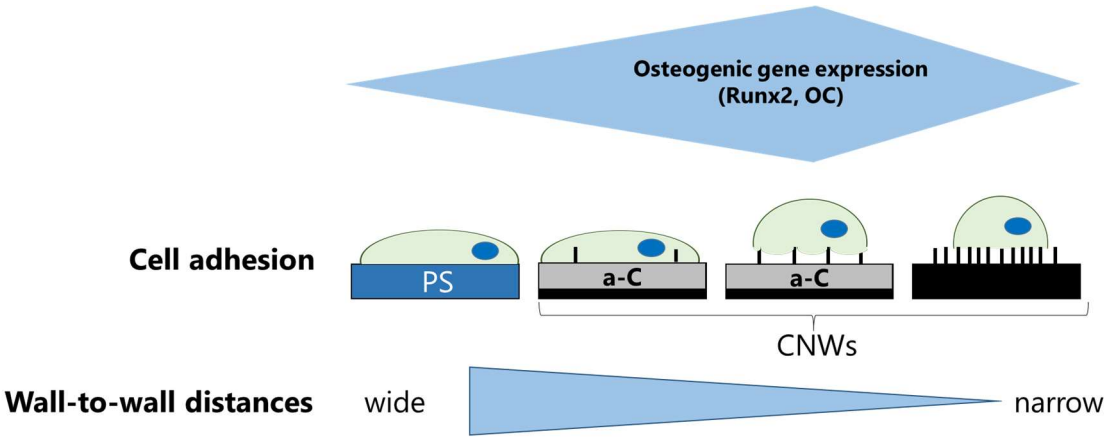

Fig. 6.4.1 An illustrative summary of the activation pathway of the osteogenic differentiation of Saos-2 cells using the isolated CNW scaffolds for cell culture.

6.5 Conclusion of this chapter

Osteogenic Saos-2 cells were incubated on CNW scaffolds with different wall-to-wall distances (D = 3300, 700, and 100 nm) synthesized using the RI-PECVD system with application of nanosecond pulses by an IES circuit. Expression of the osteogenic genes Runx2 and OC was promoted using CNWs with D = 700 nm. Isolated CNW scaffolds have potential for the control of bone generation in regenerative medicine.

Chapter 7 Conclusion and future perspectives

7.1 Summary of the thesis

In this thesis, the effect of CNWs scaffold on culturing osteoblasts are investigated. Unique morphology of cells adhered on the CNWs edge and availability of electrical stimulation due to high conductivity is suitable characteristics for the scaffold application. From the results of culturing cells on CNWs, controllability of proliferation and differentiation of osteoblasts by adjusting scaffold structure and ES was indicated. The brief summaries of chapters are explained in below.

In Chapter 1, backgrounds of carbon nanomaterials and the methods of culturing cells were explained. Characteristics on carbon materials including CNWs and their applications for scaffold are explained, and the explanations about the problem of controlling cells behavior were described. Finally, the objective and composition of thesis was described.

In Chapter 2, the explanations about experimental setup and evaluation methods were described. The synthesis methods and descriptions about the CNWs deposition chamber, i.e. radical injection plasma enhanced chemical vapor deposition system are shown. Then the methods for evaluating morphological and crystallographic characteristics of CNWs are explained. Finally, the method of culturing cells and evaluation method of cells after culturing were described.

In Chapter 3, the effect of electrical stimulation on proliferation and bone formation of cells cultured on CNWs scaffolds were described. It was found that the proliferation and nodule formation were promoted in the case of cells cultured on a CNW scaffold with electrical stimulation although bone formation was suppressed. Also, the CNWs structure on cells adhesion was observed by SEM, the shape of cells was influenced by the structure of the CNWs, and the cells were adhered on the adhesive surface only to the edge of the CNWs. In this chapter, the effect of CNWs with ES on proliferation and bone formation is clarified at the first time and the knowledge for their application were shown.

In Chapter 4, gene expression of cells incubated with ES on CNWs scaffolds with different wall-to-wall distances were described. When cultured on CNWs of

different densities, the cells proliferated in the same manner, but the morphology and the degree of differentiation of the cells were different. As the wall spacing increased, the amount of F actin at the cell edge decreased and the expression levels of Runx2 and OC increased. In addition, when cultured on CNWs having different densities by applying electrical stimulation, the cell proliferation rate and the morphology of the cell group were different. Even if the culture was performed by applying electrical stimulation on CNWs with narrower wall-to-wall distances, no effect of promoting growth was observed as compared with the culture without electrical stimulation, but on CNWs with wider wall-to-wall distances, a growth promoting effect of 58% was obtained as compared with the culture without electrical stimulation, and it was confirmed that the cell group also formed more aggregates and grew. In this chapter, the effect of wall-to-wall distances of CNWs on proliferation and differentiation is clarified at the first time.

In Chapter 5, synthesis of sparsely isolated CNWs by high-voltage nanosecond pulses application in CH_4/H_2 RI-PECVD was described. the high-voltage nanosecond pulse application inhibited the wall growth, owing to enhance adsorption of carbon atom and regulate surface diffusion lengths. As the result, the growth at the tips or edges of CNW was regulated to form the sparse CNW films. The changes of the wall-to-wall distances of CNWs films were realized under the high-voltage nanosecond pulse applications. Furthermore, this study established the novel processing for deposition by the low-pressure plasma with high-voltage nanosecond pulse. The method of controlling wall density of CNWs films is expected to utilize for realizing nanographene applications.

In Chapter 6, the effect of scaffolds with isolated CNWs on gene expression of cells was described. Osteogenic Saos-2 cells were incubated on CNW scaffolds with different wall-to-wall distances (D = 3300, 700, and 100 nm) synthesized using the RIPECVD system and application of nanosecond pulses by an IES circuit. Gene expression of the osteogenic genes Runx2 and OC was promoted using CNWs with D = 700 nm. In this chapter, the isolated CNWs scaffolds have potential for the control of bone generation in regenerative medicine.

7.2 Future perspectives

The author found that the CNWs scaffold have the effect of promoting differentiation of osteoblast-like cells and proliferation of cells were promoted by ES. What is needed for future development on utilization of CNWs for scaffold applications are the more detailed analysis on the interactions between cells and CNWs. It needs to elucidate the mechanism of cell proliferation promoted by specific electrical stimulation by measuring the membrane potential of the cell membrane and observing changes in signal transduction. In addition, it is necessary to elucidate the mechanism by which the CNWs scaffold changed the morphology of cell adhesion and promoted differentiation by evaluating the details of gene expression and signal transduction.

Also, the author found that synthesis method of synthesis of sparsely isolated CNWs by high-voltage nanosecond pulses application in the CH_4/H_2 PECVD. It was revealed that when the IES circuit connected to the stage electrode and applied high-voltage nanosecond pulses, the CNW films were sparsely grown with widely averaged wall-to-wall distances by changing the stored electrostatic powers. For elucidating the synthesis mechanism, it is important to elucidate the behavior of plasma when high-voltage nanosecond pulses are applied, but the behavior of radicals, ions and electron densities in plasma on the order of microseconds has not been elucidated.

References

1) S. H. Ku, M. Lee and C. B. Park, Adv. Healthc. Mater. **2** [2], 244 (2013).
2) E. Osawa, Kagaku (in Japanese) **25**, 854 (1970).
3) H. W. Kroto, J. R. Heath, S. C. O'Brien, R. F. Curl and R. E. Smalley, Nature **318**, 162 (1985).
4) S. Iijima, Nature **354** [6348], 56 (1991).
5) S. Iijima and T. Ichihashi, Nature **363** [6430], 603 (1993).
6) D. S. Bethune, C. H. Kiang, M. S. de Vries, G. Gorman, R. Savoy, J. Vazquez and R. Beyers, Nature **363** [6430], 605 (1993).
7) Y. Wu, P. Qiao, T. Chong and Z. Shen, Adv. Mater. **14** [1], 64 (2002).
8) M. Hiramatsu, K. Shiji, H. Amano and M. Hori, Appl. Phys. Lett. **84** [23], 4708 (2004).
9) M. Hiramatsu and M. Hori, Jpn. J. Appl. Phys. **45** [6S], 5522 (2006).
10) H. Watanabe, H. Kondo, M. Hiramatsu, M. Sekine, S. Kumar, K. Ostrikov and M. Hori, Plasma Process. Polym. **10** [7], 582 (2013).
11) H. J. Cho, H. Kondo, K. Ishikawa, M. Sekine, M. Hiramatsu and M. Hori, Carbon N. Y. **68**, 380 (2014).
12) H. Watanabe, H. Kondo, Y. Okamoto, M. Hiramatsu, M. Sekine, Y. Baba and M. Hori, J. Phys. D. Appl. Phys. **68** [26], 244105 (2014).
13) S. Kondo, H. Kondo, M. Hiramatsu, M. Sekine and M. Hori, Appl. Phys. express **3** [4], 45102 (2010).
14) K. Shiji, M. Hiramatsu, A. Enomoto, M. Nakamura, H. Amano and M. Hori, Diam. Relat. Mater. **14** [3–7], 831 (2005).
15) S. Kawai, S. Kondo, W. Takeuchi, H. Kondo, M. Hiramatsu and M. Hori, Jpn. J. Appl. Phys. **49** [6R], 60220 (2010).
16) W. Takeuchi, H. Kondo, T. Obayashi, M. Hiramatsu and M. Hori, Appl. Phys. Lett. **98** [12], 123107 (2011).
17) A. Malesevic, R. Kemps, A. Vanhulsel, M. P. Chowdhury, A. Volodin and C. Van Haesendonck, J. Appl. Phys. **104** [8], 84301 (2008).
18) W. Takeuchi, M. Ura, M. Hiramatsu, Y. Tokuda, H. Kano and M. Hori, Appl. Phys. Lett. **92** [21], 213103 (2008).
19) S. Kondo, S. Kawai, W. Takeuchi, K. Yamakawa, S. Den, H. Kano, M. Hiramatsu and M. Hori, J. Appl. Phys. **106** [9], 94302 (2009).
20) S. Imai, H. Kondo, H. Cho, H. Kano, K. Ishikawa, M. Sekine, M. Hiramatsu, M. Ito and M. Hori, J. Phys. D. Appl. Phys. **50** [40], 40LT01 (2017).
21) M. Tomatsu, M. Hiramatsu, J. S. Foord, H. Kondo, K. Ishikawa, M. Sekine, K. Takeda and M. Hori, Jpn. J. Appl. Phys. **56** [6S2], 06HF03 (2017).
22) H. W. Sampson, Alcohol. Clin. Exp. Res. **21** [3], 400 (1997).
23) K. Laitinen and M. Välimäki, Calcif. Tissue Int. **49** [1], S70 (1991).
24) P. D. Broulik and J. Ja\vráb, Horm. Metab. Res. **25** [04], 219 (1993).
25) M. Abate, D. Vanni, A. Pantalone and V. Salini, Muscles. Ligaments Tendons J. **3** [2], 63 (2013).
26) F. Oury, L. Khrimian, C. A. Denny, A. Gardin, A. Chamouni, N. Goeden, Y. Huang, H. Lee, P. Srinivas, X.-B. Gao, S. Suyama, T. Langer, J. J. Mann, T. L. Horvath, A. Bonnin and G. Karsenty, Cell **155** [1], 228 (2013).

27) P. Mera, K. Laue, J. Wei, J. M. Berger and G. Karsenty, Mol. Metab. **5** [10], 1042 (2016).
28) M. Nikkhah, F. Edalat, S. Manoucheri and A. Khademhosseini, Biomaterials **33** [21], 5230 (2012).
29) Y. Wang, M. Yao, J. Zhou, W. Zheng, C. Zhou, D. Dong, Y. Liu, Z. Teng, Y. Jiang, G. Wei and others, Biomaterials **32** [28], 6737 (2011).
30) J. Ma, X. He and E. Jabbari, Ann. Biomed. Eng. **39** [1], 14 (2011).
31) B. Bakhshandeh, M. Soleimani, N. Ghaemi and I. Shabani, Acta Pharmacol. Sin. **32** [5], 626 (2011).
32) S. Namgung, K. Y. Baik, J. Park and S. Hong, ACS Nano **5** [9], 7383 (2011).
33) M. Guvendiren and J. A. Burdick, Biomaterials **31** [25], 6511 (2010).
34) S. Huang and D. E. Ingber, Nat. Cell Biol. **1** [5], E131 (1999).
35) A. J. Engler, S. Sen, H. L. Sweeney and D. E. Discher, Cell **126** [4], 677 (2006).
36) J. S. Park, J. S. Chu, A. D. Tsou, R. Diop, Z. Tang, A. Wang and S. Li, Biomaterials **32** [16], 3921 (2011).
37) A. S. Rowlands, P. A. George and J. J. Cooper-White, Am. J. Physiol. Physiol. **295** [4], C1037 (2008).
38) J. F. Connolly, H. Hahn and O. M. Jardon, Clin. Orthop. Relat. Res. [124], 97 (1977).
39) J. A. Ogden and W. O. Southwick, Skeletal Radiol. **6** [3], 187 (1981).
40) C. T. Brighton, G. T. Tadduni, S. R. Goll and S. R. Pollack, J. Orthop. Res. **6** [5], 676 (1988).
41) Y. H. Lee, J. H. Rah, R. W. Park and C. Il Park, Yonsei Med. J. **42** [2], 194 (2001).
42) R. J. Midura, M. O. Ibiwoye, K. A. Powell, Y. Sakai, T. Doehring, M. D. Grabiner, T. E. Patterson, M. Zborowski and A. Wolfman, J. Orthop. Res. **23** [5], 1035 (2005).
43) Y. S. Shayesteh, B. Eslami, M. M. Dehghan, H. Vaziri, M. Alikhassi, A. Mangoli and A. Khojasteh, J. Prosthodont. Implant. Esthet. Reconstr. Dent. **16** [5], 337 (2007).
44) H.-P. Wiesmann, M. Hartig, U. Stratmann, U. Meyer and U. Joos, Biochim. Biophys. Acta (BBA)-Molecular Cell Res. **1538** [1], 28 (2001).
45) B. Ercan and T. J. Webster, Int. J. Nanomedicine **3** [4], 477 (2008).
46) P. R. Supronowicz, P. M. Ajayan, K. R. Ullmann, B. P. Arulanandam, D. W. Metzger and R. Bizios, J. Biomed. Mater. Res. An Off. J. Soc. Biomater. Japanese Soc. Biomater. Aust. Soc. Biomater. Korean Soc. Biomater. **59** [3], 499 (2002).
47) S. Meng, Z. Zhang and M. Rouabhia, J. Bone Miner. Metab. **29** [5], 535 (2011).
48) E. C. Stancu, A.-M. Stanciuc, S. Vizireanu, C. Luculescu, L. Moldovan, A. Achour and G. Dinescu, J. Phys. D. Appl. Phys. **47** [26], 265203 (2014).
49) M. Hiramatsu and M. Hori, *Carbon nanowalls: synthesis and emerging applications* (Springer Science \& Business Media, 2010).
50) S. Kondo, M. Hori, K. Yamakawa, S. Den, H. Kano and M. Hiramatsu, J. Vac. Sci. \& Technol. B Microelectron. Nanom. Struct. Process. Meas. Phenom. **26** [4], 1294 (2008).
51) S. Kurita, A. Yoshimura, H. Kawamoto, T. Uchida, K. Kojima, M. Tachibana, P. Molina-Morales, H. Nakai, Z. H. Ni, H. M. Fan, Y. P. Feng, Z. X. Shen, B. J. Yang and Y. H. Wu, J. Chem. Phys. **124** [10], 204703 (2005).

52) Z. H. Ni, H. M. Fan, Y. P. Feng, Z. X. Shen, B. J. Yang and Y. H. Wu, J. Chem. Phys. **124** [20], 204703 (2006).
53) D. D. Dunigan, S. B. Waters and T. C. Owen, Biotechniques **19** [4], 640 (1995).
54) N. Nomura, M. Yano, S. Katsuki, H. Akiyama, K. Abe and S. Abe, IEEE Trans. Dielectr. Electr. Insul. **16** [5], 1288 (2009).
55) M. Dijak, D. L. Smith, T. J. Wilson and D. C. W. Brown, Plant Cell Rep. **5** [6], 468 (1986).
56) I. Ermolina, Y. Polevaya, Y. Feldman, B.-Z. Ginzburg and M. Schlesinger, IEEE Trans. Dielectr. Electr. Insul. **8** [2], 253 (2001).
57) R. S. Weinstein, R. L. Jilka, M. Almeida, P. K. Roberson and S. C. Manolagas, Endocrinology **151** [6], 2641 (2010).
58) B. Sen, Z. Xie, G. Uzer, W. R. Thompson, M. Styner, X. Wu and J. Rubin, Stem Cells **33** [10], 3065 (2015).
59) J. Zhao, M. Shaygan, J. Eckert, M. Meyyappan and M. H. Rümmeli, Nano Lett. **14** [6], 3064 (2014).
60) O. Baranov, I. Levchenko, S. Xu, J. W. M. Lim, U. Cvelbar and K. Bazaka, 2D Mater. **5** [4], 44002 (2018).
61) I. Levchenko, U. Cvelbar and M. Keidar, Graphene **5** [2], 81 (2016).
62) M. Y. Pustylnik, L. Hou, A. V Ivlev, L. M. Vasilyak, L. Couëdel, H. M. Thomas, G. E. Morfill and V. E. Fortov, Phys. Rev. E **87** [6], 63105 (2013).
63) R. Hironaka, M. Watanabe, E. Hotta, A. Okino, M. Maeyama, K.-C. Ko and N. Shimizu, IEEE Trans. Plasma Sci. **28** [5], 1524 (2000).
64) K. Takaki, I. Yagi, T. Fujiwara and T. Go, IEEE Trans. Dielectr. Electr. Insul. **18** [5], 1752 (2011).
65) L. Jia, H. Sugiura, H. Kondo, K. Takeda, K. Ishikawa, O. Oda, M. Sekine, M. Hiramatsu and M. Hori, Jpn. J. Appl. Phys. **55** [4], 40305 (2016).
66) H. Sugiura, L. Jia, H. Kondo, K. Ishikawa, T. Tsutsumi, T. Hayashi, K. Takeda, M. Sekine and M. Hori, Jpn. J. Appl. Phys. **57** [6S2], 06JE03 (2018).
67) H. Sugiura, L. Jia, Y. Ohashi, H. Kondo, K. Ishikawa, T. Tsutsumi, T. Hayashi, K. Takeda, M. Sekine and M. Hori, Jpn. J. Appl. Phys. **58** [3], 30912 (2019).
68) X. Z. X. Zhao, T. O. T. Okazaki, A. K. A. Kasuya, H. S. H. Shimoyama and Y. A. Y. Ando, Jpn. J. Appl. Phys. **38** [10R], 6014 (1999).
69) Y. S. Y. Saito and M. I. M. Inagaki, Jpn. J. Appl. Phys. **32** [7A], L954 (1993).
70) S. Suzuki, A. Chatterjee, C.-L. Cheng and M. Yoshimura, Jpn. J. Appl. Phys. **50** [1S1], 01AF08 (2011).
71) S. D. Stoica, S. Vizireanu, T. Acsente and G. Dinescu, Plasma Chem. Plasma Process. **38** [4], 695 (2018).
72) S. Vizireanu, S. D. Stoica, C. Luculescu, L. C. Nistor, B. Mitu and G. Dinescu, Plasma Sources Sci. Technol. **19** [3], 34016 (2010).
73) N. Gupta and S. C. Sharma, Phys. Plasmas **25** [7], 73509 (2018).
74) K. Lehmann, O. Yurchenko, J. Melke, A. Fischer and G. Urban, Electrochim. Acta **269**, 657 (2018).
75) S. Ghosh, K. Ganesan, S. R. Polaki, T. Mathews, S. Dhara, M. Kamruddin and A. K. Tyagi, Appl. Surf. Sci. **349**, 576 (2015).
76) S. Ghosh, K. Ganesan, S. R. Polaki, T. R. Ravindran, N. G. Krishna, M. Kamruddin and A. K. Tyagi, J. Raman Spectrosc. **45** [8], 642 (2014).

77) K. K. Mishra, S. Ghosh, T. R. Ravindran, S. Amirthapandian and M. Kamruddin, J. Phys. Chem. C **120** [43], 25092 (2016).
78) S. Ghosh, S. R. Polaki, N. G. Krishna and M. Kamruddin, J. Mater. Sci. **53** [10], 7316 (2018).
79) S. Ghosh, S. R. Polaki, N. Kumar, S. Amirthapandian, M. Kamruddin and K. K. Ostrikov, Beilstein J. Nanotechnol. **8** [1], 1658 (2017).
80) C. Y. Cheng and K. Teii, IEEE Trans. Plasma Sci. **40** [7], 1783 (2012).
81) C. Y. Cheng, M. Nakashima and K. Teii, Diam. Relat. Mater. **27**, 40 (2012).
82) M. Zhu, J. Wang, B. C. Holloway, R. A. Outlaw, X. Zhao, K. Hou, V. Shutthanandan and D. M. Manos, Carbon N. Y. **45** [11], 2229 (2007).
83) G. Filipič, O. Baranov, M. Mozetič and U. Cvelbar, J. Appl. Phys. **117** [4], 43304 (2015).
84) A. Giese, S. Schipporeit, V. Buck and N. Wöhrl, Beilstein J. Nanotechnol. **9** [1], 1895 (2018).
85) T. Ozdemir, D. T. Bowers, X. Zhan, D. Ghosh and J. L. Brown, Sci. Rep. **9** [1], 1 (2019).
86) P. Rougerie, R. dos Santos, M. Farina and K. Anselme, Appl. Sci. **11** [4], 1791 (2021).
87) S. Kumar, S. Raj, E. Kolanthai, A. K. Sood, S. Sampath and K. Chatterjee, ACS Appl. Mater. \& interfaces **7** [5], 3237 (2015).
88) J. Hasan, S. Jain and K. Chatterjee, Sci. Rep. **7** [1], 1 (2017).

Acknowledgement

The present research was performed in the Hori and Ishikawa laboratory, the department of electronic engineering, Nagoya University. Author would like to appreciate his research advisor, Professor Masaru Hori, the center for low-temperature plasma sciences, Nagoya University, for his guidance, advice, and encouragements through the course of this research. The author also would like to greatly appreciate his vice-advisers, Professor Noriyasu Ohno, Professor Tomokazu Fukutsuka, the department of electrical engineering, Nagoya University, Professor Hirotaka Toyoda, the department of electronic engineering, Nagoya University and Professor Masafumi Jinno, the department of electrical and electronic engineering, Ehime University for their guidance and valuable suggestions in preparing this thesis.

The author thanks enormous grateful to Professor Kenji Ishikawa and Associate Professor Hiroki Kondo, the center for low-temperature plasma sciences, Nagoya University, for lots of valuable comments in proceeding daily researches. The author sincerely thanks Professor Hiromasa Tanaka, Professor Naohiro Shimizu, Professor Makoto Sekine, and Assistant Professor Takayoshi Tsutsumi, the center of low-temperature plasma sciences, Nagoya University, Professor Mineo Hiramatsu, Associate Professor Keigo Takeda, the department of electrical and electronic engineering, Meijo University, for the useful advice in the researches. The author also would like to thanks Professor Masafumi Ito, Professor Takayuki Ohta, the department of electrical and electronic engineering, Meijo University, Professor Osamu Oda, Professor Toshio Hayashi, and Lecturer Hiroshi Hashizume, the center of low-temperature plasma sciences, Nagoya University, for their valuable comments and suggestions.

The author also thanks sincerely Dr. Zecheng Liu, Dr. Naoyuki Kurake, Dr. Atsushi Ando, Dr. Tomoki Amano, Dr. Yan Zhang, Dr. Takashi Kako, Dr. Kuangda Sun, Dr. Timothy Ryan Brubaker, Dr Shun Imai, Dr. Hirotsugu Sugiura, Dr. Masakazu Tomatsu, Dr. Yusuke Fukunaga, Dr. Borude Ranjit Rohidas, Mr. Atsuki Asano, Mr. Shunichi Sato, Mr. Shinnosuke Takai, Mr. Suiki Tanaka, Mr. Takuya Tonami, Mr. Kenichi Naito, Mr. Ryo Furuta, Mr. Naoki Yoshitake, Mr. Masato Imamura, Mr. Toshinari Ueyama, Mr. Daiki Kanno, Mr. Ren Kuramashi, Mr. Yukihiro Kurokawa, Ms. Mika Takahashi, Ms. Moe Okabe, Mr. Xitong Xie, Ms. Yao Han, Ms. Kaede Katsuno, Mr. Naoki Takeda, Mr. Yugo Hosoi, Mr. Kaito Murakami, Mr. Soutarou Yamaoka, Mr. Yasuyuki Ohashi, Mr. Takahiro

Omichi, Mr. Takumi Kato, Mr. Kazuya Nakane, Mr. Masaki Hasegawa, Mr. Ryo Hamaji, Mr. Shogo Maeda, Mr. Ni Jiawei, Ms. Liu Yang, Mr. Atsushi Ozaki, Mr. Yuki Suda, Mr. Ryusei Sakai, Mr. Masahiro Hazumi, Mr. Shogo Matsumura, Mr. Tatsuyuki Moriyama, and all other students who have studied in the Hori and Ishikawa Laboratory for giving the big pleasure in life and creating a most enjoyable work atmosphere.

The author appreciates Ms. Yoko Kuwabara, Ms. Kazuyo Hirota, Ms. Taeko Terasawa, Ms. Aya Honda, Kanae Teshigawara and Asako Nishiyama, for lots of encouragements and helpful advices in day-to-day life.

Finally, the author would like to appreciate his family including Mr. Tatsuya Ichikawa, Ms. Yoko Ichikawa, his grandparents, uncles, aunts, and cousins, for their help, support, and encouragement.

List of papers

I. Original papers		
Title	Journal	Authors
1. Effect of electrical stimulation on proliferation and bone-formation by osteoblast-like cells cultured on carbon nanowalls scaffolds	Applied Physics Express **12**,2,025006 pp.1-4 (2019)	Tomonori Ichikawa, Suiki Tanaka, Hiroki Kondo, Kenji Ishikawa, Takayoshi Tsutsumi, Makoto Sekine, and Masaru Hori
2. Gene expression of osteoblast-like cells incubated on carbon-nanowall scaffolds with different wall-to-wall distances and electrical stimulation	ACS Appl. Bio Mater. **2**, 7, pp. 2698–2702 (2019)	Tomonori Ichikawa, Hiroki Kondo, Kenji Ishikawa, Takayoshi Tsutsumi, Hiromasa Tanaka, Makoto Sekine, and Masaru Hori
3. Synthesis of isolated carbon nanowalls via high-voltage nanosecond pulses in conjunction with CH_4/H_2 plasma enhanced chemical vapor deposition	Carbon **161**, pp. 403-412 (2020).	Tomonori Ichikawa, Naohiro Shimizu, Kenji Ishikawa, Mineo Hiramatsu, and Masaru Hori
4. Scaffolds with isolated carbon nanowalls promote osteogenic differentiation through Runt-related transcription factor 2 and osteocalcin gene expression of osteoblast-like cells	AIP Advances **12**, 025216 pp.1-6 (2022).	Tomonori Ichikawa, Kenji Ishikawa, Hiromasa Tanaka, Naohiro Shimizu, and Masaru Hori

II. International Conferences		
Title	Journal	Authors
1. Effect of shape and conductivity of carbon nanowalls scaffold on cell morphology and proliferation	Workshop on advanced plasma applications on bio and nanomaterials, Nagoya University, Aichi, Japan, January 27, 2017	Tomonori Ichikawa, Suiki Tanaka, Hiroki Kondo, Hiroshi Hashizume, Hiromasa Tanaka, Kenji Ishikawa, Makoto Sekine, Masaru Hori
2. A novel controlling method of differentiation of cultured cells on carbon nanowalls scaffold with an electric stimulation	The 11th Asian-European International Conference on Plasma Surface Engineering, (Jeju Island, Korea, September 11-15, 2017), S7-OR03	Tomonori Ichikawa, Suiki Tanaka, Hiroki Kondo, Kenji Ishikawa, Hiroshi Hasizume, Hiromasa Tanaka, and Masaru Hori
3. Regulation of cell proliferation changing duty ratio of an electrical stimulation on carbon nanowalls scaffold	11th International Symposium on Advanced Plasma Science and its Application for Nitrides and Nanomaterials/12th International Conference on Plasma-Nano Technology & Science (ISPlasma 2019/IC-PLANTS 2019) Nagoya Institute of Technology, Nagoya, Japan. March 17-21, 2019. 19P4-39 Mar 19	Tomonori Ichikawa, Hiroki Kondo, Hiroshi Hashizume, Hiromasa Tanaka, Takayoshi Tsutsumi, Kenji Ishikawa, Makoto Sekine, and Masaru Hori
4. Nanosecond high-voltage pulse imposed chemical vapor deposition (ns HV CVD) of sparsely isolated carbon nanowalls	INTERFINISH 2020(Online, September 6-8 2021) 5035	Tomonori Ichikawa, Kenji Ishikawa, Naohiro Shimizu, and Masaru Hori